



*IN-02
29-4-61*

TECHNICAL MEMORANDUM

X-215

EFFECT OF AFTERBODY TERMINAL FAIRINGS ON THE PERFORMANCE
OF A PYLON-MOUNTED TURBOJET-NACELLE MODEL

By Conrad M. Willis and Charles E. Mercer

Langley Research Center
Langley Field, Va.

Declassified March 15, 1962

NATIONAL AERONAUTICS AND SPACE ADMINISTRATION
WASHINGTON

March 1960

NATIONAL AERONAUTICS AND SPACE ADMINISTRATION

TECHNICAL MEMORANDUM X-215

EFFECT OF AFTERBODY TERMINAL FAIRINGS ON THE PERFORMANCE
OF A PYLON-MOUNTED TURBOJET-NACELLE MODEL*

By Conrad M. Willis and Charles E. Mercer

SUMMARY

An investigation of the effect of afterbody terminal fairings on the performance of a pylon-mounted turbojet-nacelle model has been conducted in the Langley 16-foot transonic tunnel. A basic afterbody having a boattail angle of 16° was investigated with and without terminal fairings. The equivalent boattail angle, based on the cross-sectional area of the afterbody and terminal fairings, was 8° . Therefore, a simple body of revolution with a boattail angle of 8° was included for comparison. The tests were made at an angle of attack of 0° , Mach numbers of 0.80 to 1.05, jet total-pressure ratio of 1 to approximately 5, and an average Reynolds number per foot of 4.1×10^6 . A hydrogen peroxide jet simulator was used to supply the hot-jet exhaust.

The results indicate that addition of terminal fairings to a 16° boattail afterbody increased the thrust-minus-drag coefficients and provided the lowest effective drag of the three configurations tested.

INTRODUCTION

Optimum performance of a nozzle-exit—afterbody combination at both subsonic and supersonic speeds requires continuously variable internal and external surfaces. Such variable geometry configurations result in complexity of fabrication and weight penalty. In previous attempts to circumvent these problems, simple semifixed geometry configurations have been designed that perform well at high speeds. Predominant among these configurations has been the fixed convergent-divergent ejector with variable primary-nozzle and secondary air flow (refs. 1 to 3). However, these configurations show sizable performance losses when operated at off-design conditions. The use of terminal fairings as a new approach to the solution of this problem was introduced in reference 4. The

*Title, Unclassified.

basis for this concept of design is the interaction of the internal and external flows in the afterbody jet-exit region. The results of a previous investigation related to this subject have been reported in reference 5. A terminal-fairing configuration consists of a multiplicity of streamlined bodies clustered around the afterbody and extending downstream of the jet exit and spaced so as not to form a complete barrier between jet and external flow.

Because of the complex nature of the mixing flows around the terminal bodies or fairings, changes in afterbody boattailing and the arrangement and shape of the fairings may have appreciable effects on the performance of nacelles with this type of afterbody-nozzle combination. The terminal fairings of reference 5 consisted of six bodies of circular cross section on an afterbody with a boattail angle of about 16° . The present paper reports results of a continuation of the investigation of terminal fairings; however, the terminal fairings consisted of only four bodies of flattened cross-sectional shape. The performance of a simple body with 16° boattail angle is compared with that of the same afterbody having the four terminal fairings added. These added bodies produced a configuration having an area equivalent to a body of revolution with an 8° boattail angle (a near-optimum value). A simple body of revolution having a boattail angle of 8° was also tested to provide a further comparison. All configurations were tested with a nonafterburning type primary nozzle.

This investigation was conducted in the Langley 16-foot transonic tunnel over a Mach number range of 0.80 to 1.05 at 0° angle of attack. Jet total-pressure ratio was varied from 1 (jet off) to approximately 5 at each Mach number. The effects of secondary air on the terminal-fairing configuration and a comparable body of revolution were investigated at a Mach number of 0.90 and a jet total-pressure ratio of 4; the corrected secondary-to-primary weight-flow ratios varied from 0 (no flow) to about 0.06. The turbojet exhaust was simulated by a hydrogen peroxide hot-jet unit similar to that described in reference 6.

SYMBOLS

A	cross-sectional area, sq ft
C_D	drag coefficient
C_D'	effective drag coefficient, $C_{F,p} - (C_F - C_D)$
$C_{D,a}$	afterbody pressure-drag coefficient, $-\sum \frac{C_p A_i}{A_{max}}$

C_F	thrust coefficient
$C_F - C_D$	thrust-minus-drag coefficient, $\frac{F - D}{qA_{\max}}$
$C_{F,ej}$	ejector jet thrust coefficient, $\frac{F_{ej}}{qA_{\max}}$
$C_{F_i,c}$	ideal convergent-nozzle jet thrust coefficient, $\frac{F_{i,c}}{qA_{\max}}$
$C_{F,p}$	primary-nozzle jet thrust coefficient, $\frac{F_p}{qA_{\max}}$
C_p	pressure coefficient, $\frac{p_l - p_\infty}{q}$
D	drag, lb
d	diameter, in.
F	thrust, lb
$F - D$	thrust minus drag, $F_{bal} - D_{bal} + (A_{s,2} - A_{s,1})(p_1 - p_2)$, lb
F_{ej}	ejector jet thrust, $F_p + \frac{w_s}{g} V_3 + (p_3 - p_\infty)(A_s - A_p) + \int_{A_s}^{A_e} (p_l - p_\infty) dA$, lb
$F_{i,c}$	ideal convergent-nozzle jet thrust, $\frac{w_p}{g} \sqrt{\gamma g R \frac{2}{\gamma + 1} T_{t,j}} + A_p(p_p - p_\infty)$, lb
F_p	primary-nozzle thrust, lb
g	acceleration due to gravity, ft/sec ²
l	afterbody length, in.
L	distance from primary nozzle to afterbody exit, in.
M	free-stream Mach number

4

p	static pressure, lb/sq ft
P_t	total pressure, lb/sq ft
$P_{t,j}/P_\infty$	jet-pressure ratio (ratio of primary jet total pressure to free-stream static pressure)
q	dynamic pressure, lb/sq ft
R	gas constant, ft/°R
T_t	stagnation temperature, °F
V	velocity, ft/sec
w	weight flow rate, lb/sec
$\frac{w_s}{w_p} \sqrt{\frac{T_{t,s}}{T_{t,p}}}$	corrected secondary-to-primary weight-flow ratio
x	axial distance from reference stations (see figs. 1 and 3), positive rearward, in.
y	radial coordinate, in.
γ	ratio of specific heats
β	boattail angle of afterbody base, deg
θ	meridian angle of model, deg

Subscripts:

bal	balance
e	exit of afterbody
eqv	equivalent
j	jet
l	local
max	maximum
p	primary nozzle

s	seal or secondary air
∞	free-stream conditions
1	forward compartment of model
2	outer compartment of model
3	rear compartment of model

APPARATUS AND PROCEDURE

Wind Tunnel and Model Support System

The investigation was conducted in the Langley 16-foot transonic tunnel, which is an octagonal slotted-throat single-return wind tunnel operated at atmospheric stagnation pressures. The model was supported by a sweptback pylon attached to a conventional sting 18 inches below the model center line as shown in figure 1. Since the model pylon is similar to actual installations and since the same support was used for all configurations, no corrections were made for support interference. Interference effects for this mounting system are discussed in reference 7.

Nacelle and Balance System

A sketch of the nacelle model is presented in figure 1, and a photograph of the nacelle and pylon is shown in figure 2. The nacelle shell and jet simulator unit were separate systems and each was attached to the pylon by its own balance. The hydrogen peroxide jet simulator (described in ref. 6) had an exhaust temperature of about 1,350° F. Secondary air was exhausted into an annular passage between the tail-pipe and nacelle shell.

Configurations

The three afterbody configurations (fig. 3) were designed for the purpose of evaluating the relative performance of: a basic axisymmetric boattailed afterbody (configuration I), the same afterbody with terminal fairings added to reduce the effective boattail angle (configuration II), and a simple afterbody having axisymmetric boattailing equivalent to that determined by the axial distribution of cross-sectional area of the terminal-fairing configuration (configuration III). All these afterbodies had diameter ratios (jet nozzle to maximum nacelle and base to

maximum nacelle) that corresponded to those for typical turbojet-nacelle installations with primary nozzles in the nonafterburning condition. The afterbodies were detachable at the 47.125-inch station.

Dimensions of configuration I, the basic 16° boattail, are shown in the sketch presented as figure 3(a). Configuration II (fig. 3(b)) was formed by adding four detachable terminal fairings to configuration I. The fairings were of flattened cross-sectional shape and were designed to provide an equivalent boattail angle of 8° . This angle was arbitrarily defined as the boattail angle produced by distributing the cross-sectional area of the four fairings in an annulus around the basic boattail and was measured at the 57.030-inch afterbody exit station. Configuration III (fig. 3(c)) is representative of a low-drag afterbody in the transonic speed range (ref. 8). The low boattail angle necessitated an extension in afterbody length to achieve a base area approximately the same as the other two configurations (figs. 4 and 5). Configuration III was selected for testing to provide a performance comparison between the terminal-fairing configuration and a simple body of revolution with the same boattail angle. Area distributions for configurations I, II, and III are shown in figure 5.

Instrumentation

External and internal static pressures were measured on the afterbodies at locations shown in figure 3. It should be noted that for configurations I and II there is only one row of external pressure orifices which is on the top of the afterbody. In addition, primary jet total pressures, secondary air exit static pressures, and primary and secondary total temperatures were measured. (See fig. 6.) The pressure tubing from each orifice was conducted out of the nacelle through the pylon support and connected to an electrical pressure transducer located in the sting barrel. The electrical pressure transducers were manifolded to a common reference pressure and the whole transducer manifold system was held at a constant temperature to keep both the zero and sensitivity shifts of the transducers to a minimum. Electrical signals from the pressure transducers were transmitted to carrier amplifiers and then to recording oscillographs located in the tunnel control room.

The thrust forces of the jet simulator were obtained from a one-component thrust balance. A four-component internal balance measured the forces and moments on the nacelle; however, only the drag measurements are presented in this paper. Figure 5 indicates the balance locations and the pressures, areas, and temperatures associated with the reduction and correction of data. An electronic flowmeter and a calibrated venturi were used to measure the primary and secondary flow rates, respectively.

Data Reduction

Model data recorded by oscillograph trace deflections were used to compute standard force and pressure coefficients. Because of limited instrumentation of configurations I and II, afterbody pressure drag was not computed for these configurations.

Since thrust and drag cannot be readily separated for configurations designed to allow mixing of internal and external flows, thrust minus drag, or net propulsive force, is used to compare the three afterbodies. The processes described in reference 5 were used to obtain net propulsive force and effective drag. Ejector thrust was determined as follows for configuration III:

$$F_{ej} = F_p + \frac{w_s}{g} V_s + (p_3 - p_\infty)(A_s - A_p) + \int_{A_s}^{A_e} (p_l - p_\infty) dA$$

where

$$F_p = F_{bal} - \frac{w_s}{g} V_3 - (p_3 - p_\infty)(A_{s,2} - A_p) + (p_1 - p_\infty)A_{s,2}$$

The equation for F_p applies to all configurations. Locations of these pressures and areas are shown in figure 6.

Accuracy

Estimated accuracy of data presented in this paper is as follows:

M	±0.005
$P_{t,j}/P_\infty$	±0.10
$C_{D,a}$	±0.01
$C_{F,ej}$	±0.01
$C_F - C_D$	±0.01
C_D'	±0.01
$\frac{w_s}{w_p} \sqrt{\frac{T_{t,s}}{T_{t,p}}}$	±0.005

TESTS

All tests were conducted at 0° angle of attack. The Mach number range was from 0.80 to 1.05, and the average Reynolds number per foot

was 4.1×10^6 . Ratios of primary jet total pressure to free-stream static pressure ranged from 1 (jet off) to about 5 at each Mach number. Secondary air at flow rates of 0 to about 0.25 pound per second

$\left(\frac{w_s}{w_p} \sqrt{\frac{T_{t,s}}{T_{t,p}}} = 0 \text{ to } 0.06 \right)$ was used for tests of configurations II and III

at a Mach number of 0.90 and a jet total-pressure ratio of 4.

RESULTS

Longitudinal distributions of pressure for afterbody configuration III at pressure ratios of 1 and 5 are presented in figure 7. In figure 8, representative pressure distributions for the three afterbody configurations are compared. Figure 9 presents pressure distributions obtained over the six-body terminal-fairing configuration of reference 5 and compares these distributions with those obtained over the four-body terminal-fairing configuration of the present investigation. Afterbody pressure-drag coefficient for configuration III is presented in figure 10. Thrust data are shown in figures 11 to 13. Figures 14 and 15 present performance comparisons on a thrust-minus-drag basis. Effective drag coefficient at a scheduled jet total-pressure ratio is shown in figure 16. Thrust-minus-drag coefficients are compared for various configurations in figures 17 and 18.

DISCUSSION

Afterbody Pressure Distributions

The effect of jet operation on afterbody pressure distributions of configuration III is presented in figure 7. Jet operation increased afterbody pressures near the base. This favorable jet interference generally decreased with increasing Mach number, an effect that is typical for boattails of this shape (ref. 7).

Figure 8 presents a comparison of pressure distributions obtained from the top row of orifices for the three afterbody configurations of the present investigation. Configuration I with a boattail angle of 16° had the most negative afterbody pressures, as expected. The pressure level for the terminal-fairing configuration with an equivalent boattail angle of 8° (configuration II) generally fell about halfway between the levels for the bodies of revolution with boattail angles of 16° and 8° (configurations I and III). However, in the region near the boattail base where the orifices were located between the terminal fairings, the pressures for configuration II were more negative than those for either

of the bodies of revolution. Jet operation decreased the pressures near the base for configuration II but increased these pressures for the other two afterbodies.

In order to examine this apparently unfavorable effect of terminal fairings on the boattail base region, sample pressure distributions obtained over the six-body terminal-fairing configuration of reference 5 are shown in figure 9. The data for configuration II shown in figure 8 at a Mach number of 0.90 are repeated for comparison purposes. Although the pressure coefficients for the six-body terminal-fairing configuration were more positive than those for the four-body terminal-fairing configuration, the trends of the pressure distributions near the bases of the bodies were similar. The pressures on the surfaces of the six terminal fairings behind the base generally increased substantially with jet operation and these increased pressures resulted in thrust forces on the fairings. It would be expected that a similar pressure recovery would occur over the four terminal bodies of the present investigation.

Afterbody Pressure Drag

Afterbody pressure-drag coefficients for configuration III are shown in figure 10. Increasing the jet total-pressure ratio caused decreases in afterbody pressure-drag coefficient. Limited data showing the addition of secondary air flow at $M = 0.90$ indicated little effect on afterbody drag in this investigation. The decrease in afterbody pressure-drag coefficient indicated by the test point at the jet-off condition is probably due to a base bleed effect. Also shown in figure 10 are data for an afterbody with a boattail angle of 15° and a base-to-maximum-diameter ratio of 0.538 (afterbody II of ref. 7). It would be expected that the magnitude of the afterbody pressure-drag coefficients for the 15° boattail body of reference 7 would be approximately the same as those for the 16° boattail afterbody of the present investigation (configuration I) since both configurations were investigated on the same nacelle and support system. The difference in level of afterbody pressure-drag coefficients for the two configurations presented in figure 10 should therefore be indicative of the drag differences expected between configurations I and III of the present investigation.

Primary-Nozzle Jet Performance

The variation of primary-nozzle jet thrust coefficient with jet total-pressure ratio is presented in figure 11. The data are compared with the ideal convergent-nozzle jet thrust coefficient based on measured jet total pressure, temperature, and weight flow rates. Since the

same primary nozzle was used for all configurations, the test data should fall on a single line. Efficiency, as indicated by the ratio of primary thrust to ideal thrust, varied from approximately 0.90 at $p_{t,j}/p_{\infty} = 2$ to 0.95 at $p_{t,j}/p_{\infty} = 5$.

Ejector Thrust

In order to obtain a low boattail angle with the same base diameter as the other configurations, the afterbody of configuration III had to be extended and thereby resulted in an ejector with a greater spacing ratio. (See fig. 3(c).) This arrangement, therefore, would require a carefully programmed amount of secondary air flow if it were to operate efficiently as an ejector. Reference 9 indicates a thrust ratio of approximately 1.0 at zero secondary air flows for ejector geometries similar to configurations I and II in the pressure-ratio range of this investigation. Ejector thrust coefficient for configuration III is presented in figure 12 for zero secondary air flow. In addition, at a Mach number of 0.90, a point is presented for the maximum amount of secondary air flow available through the system. With no secondary air flow, large ejector-thrust losses occur at the higher jet total-pressure ratios. These losses are probably due to jet attachment to the shroud and low pressures in the secondary air passages. With the addition of about 6-percent corrected secondary air flow, the ejector thrust coefficients approached more closely the ideal convergent-nozzle thrust coefficient.

An indication of the ejector performance with secondary weight flow ratio may be noted from figure 13 where jet thrust ratios of configuration III and static-test data for a similar ejector (diameter ratio, 1.40; spacing ratio, 0.803) of reference 9 are compared. It can be seen that the trends with jet total-pressure ratio are similar for the two configurations at zero secondary air flow, but the losses for configuration III are much higher, probably due to the differences in the internal geometry of the secondary-flow passage and Mach number effects. With each successive increase in secondary air flow, an increase in performance was obtained with the test configuration. This increase indicated that, with sufficient secondary air flow, the ejector of configuration III would provide acceptable performance. However, these gains would be offset by the penalty for bringing this secondary air on board. The force required to bring 6-percent corrected secondary air flow to rest from the free-stream Mach number of 0.90 and $p_{t,j}/p_{\infty} = 4$ amounts to a penalty of about 0.084 in drag coefficient.

Thrust-Minus-Drag Measurements

Thrust-minus-drag measurements provide a convenient means of comparing overall performance of configurations having the same primary

nozzles. Separation of the data into the basic quantities of thrust and drag necessitates an arbitrary division of forces between the thrust and the external nacelle drag. This division becomes particularly complicated for the terminal-fairing configuration because of the ejector action of the jet bulb expanding along the inner surface and sides of the fairings.

The variation in thrust-minus-drag coefficient with jet total-pressure ratio for the three afterbody configurations is shown in figure 14. The addition of four terminal fairings to the 16° boattail body improved the model performance at all jet total-pressure ratios. Performance losses for configuration III, previously indicated by the ejector-thrust-coefficient curves of figure 12, occurred at the higher jet total-pressure ratios. With approximately 6-percent corrected secondary air flow at a Mach number of 0.90, the performance of configuration III was slightly better than that of configuration I when losses due to obtaining this flow were neglected. The addition of secondary air flow, however, had little effect on the performance of the terminal-fairing configurations.

Performance comparisons are presented in figure 15 for a typical schedule of turbojet-engine pressure ratios with Mach number. Gains of about 6 percent in thrust-minus-drag performance in the Mach number range from 0.90 to 1.00 were obtained by adding the terminal fairings to the basic body. It should be noted that thrust-minus-drag performance for configuration III is penalized by the absence of secondary air flow.

The data of figure 15 are presented in another form in figure 16 to show the variation with Mach number of the effective drag coefficients of the three configurations considered in this paper. Effective drag coefficients were obtained by subtracting the experimentally determined values of thrust-minus-drag coefficient from the computed values of primary-nozzle thrust coefficient. The data for configurations I and II show that the addition of the terminal fairings to the basic configuration reduced the effective drag 44 percent at a Mach number of 0.90 and about 21 percent at a Mach number of 1.00. Since the effective drag coefficients reflect gains or losses associated with the internal ejector arrangement as well as differences in external drag (see ref. 5), the losses in ejector thrust for configuration III (fig. 12) would show up as high effective drag coefficients. Therefore, data for configuration III without secondary flow are omitted from figure 16. A one-point comparison of the terminal-fairing and the 8° axisymmetrical boattail bodies (configurations II and III) is made at a Mach number of 0.90 to indicate the relative effective drag coefficients of the two afterbodies with a representative corrected secondary-to-primary weight flow ratio of 0.04. With this secondary air flow rate, the four-terminal-fairing model had an effective drag coefficient about 0.047 lower than that for

the 8° axisymmetrical boattail model. These results were obtained with the nonafterburning primary jet nozzle, and performance improvements due to the terminal fairings would probably be larger for afterburner nozzle operation. (See ref. 5.) Thrust-minus-drag coefficients for two terminal-fairing configurations are presented in figure 17. Since the nozzle sizes and propellant flow rates were different, the data were normalized on the basis of primary-nozzle exit area. The configuration with four terminal fairings provided better performance than the six-terminal-fairing configuration at Mach numbers above 0.95. However, all the differences shown in propulsive force are not necessarily due to the change in the number of fairings, but must be attributed to the entire afterbody arrangement.

The effect of secondary air weight flow ratio on the thrust-minus-drag coefficients of several types of terminal-fairing configurations and the comparative afterbody, configuration III, is shown in figure 18 for a Mach number of 0.90 and a jet total-pressure ratio of 4. The slotted divergent ejector included in this figure (ref. 5) is considered to also represent a type of terminal fairing in that the internal portion of the body is ventilated to the free stream beyond the primary nozzle. In general, small amounts of secondary air flow produced the most change in thrust-minus-drag coefficients. Additional increases in secondary air flow rates resulted in only small changes in thrust-minus-drag coefficients. The four-terminal-fairing configuration had higher thrust-minus-drag coefficients than the other afterbodies considered herein throughout the secondary air flow range of this investigation.

CONCLUSIONS

An investigation of the effects of afterbody terminal fairings on the performance of a pylon-mounted jet-nacelle model has been conducted in the Langley 16-foot transonic tunnel. The results have led to the following conclusions:

1. Addition of four terminal fairings to a simple 16° boattail body of revolution increased the thrust-minus-drag coefficients and decreased the effective drag coefficients over the Mach number range.
2. At Mach numbers above 0.95, the configuration with four terminal bodies had higher thrust-minus-drag coefficients (based on primary-nozzle exit area) than did the configuration with six terminal bodies of a previous investigation (NASA MEMO 10-24-5(L)).

Langley Research Center,
National Aeronautics and Space Administration,
Langley Field, Va., October 15, 1959.

REFERENCES

1. Greathouse, William K., and Beale, William T.: Performance Characteristics of Several Divergent-Shroud Aircraft Ejectors. NACA RM E55G21a, 1955.
2. Beheim, Milton A.: Off-Design Performance of Divergent Ejectors. NACA RM E58G10a, 1958.
3. Norton, Harry T., Jr., Cassetti, Marlowe D., and Mercer, Charles E.: Transonic Off-Design Performance of a Fixed Divergent Ejector Designed for a Mach Number of 2.0. NASA TM X-165, 1959.
4. Swihart, John M., Norton, Harry T., Jr., and Schmeer, James W.: Effect of Several Afterbody Modifications Including Terminal Fairings on the Drag of a Single-Engine Fighter Model With Hot-Jet Exhaust. NASA MEMO 10-29-58L, 1958.
5. Runckel, Jack F.: Preliminary Transonic Performance Results for Solid and Slotted Turbojet Nacelle Afterbodies Incorporating Fixed Divergent Jet Nozzles Designed for Supersonic Operation. NASA MEMO 10-24-58L, 1958.
6. Runckel, Jack F., and Swihart, John M.: A Hydrogen Peroxide Hot-Jet Simulator for Wind-Tunnel Tests of Turbojet-Exit Models. NASA MEMO 1-10-59L, 1959.
7. Swihart, John M., Mercer, Charles E., and Norton, Harry T., Jr.: Effect of Afterbody-Ejector Configurations on the Performance at Transonic Speeds of a Pylon-Supported Nacelle Model Having a Hot-Jet Exhaust. NASA MEMO 1-4-59L, 1959.
8. Cabbage, James M., Jr.: Jet Effects on the Drag of Conical Afterbodies for Mach Numbers of 0.6 to 1.28. NACA RM L57B21, 1957.
9. Greathouse, W. K., and Hollister, D. P.: Preliminary Air-Flow and Thrust Calibrations of Several Conical Cooling-Air Ejectors With a Primary to Secondary Temperature Ratio of 1.0. II - Diameter Ratios of 1.06 and 1.40. NACA RM E52F26, 1952.

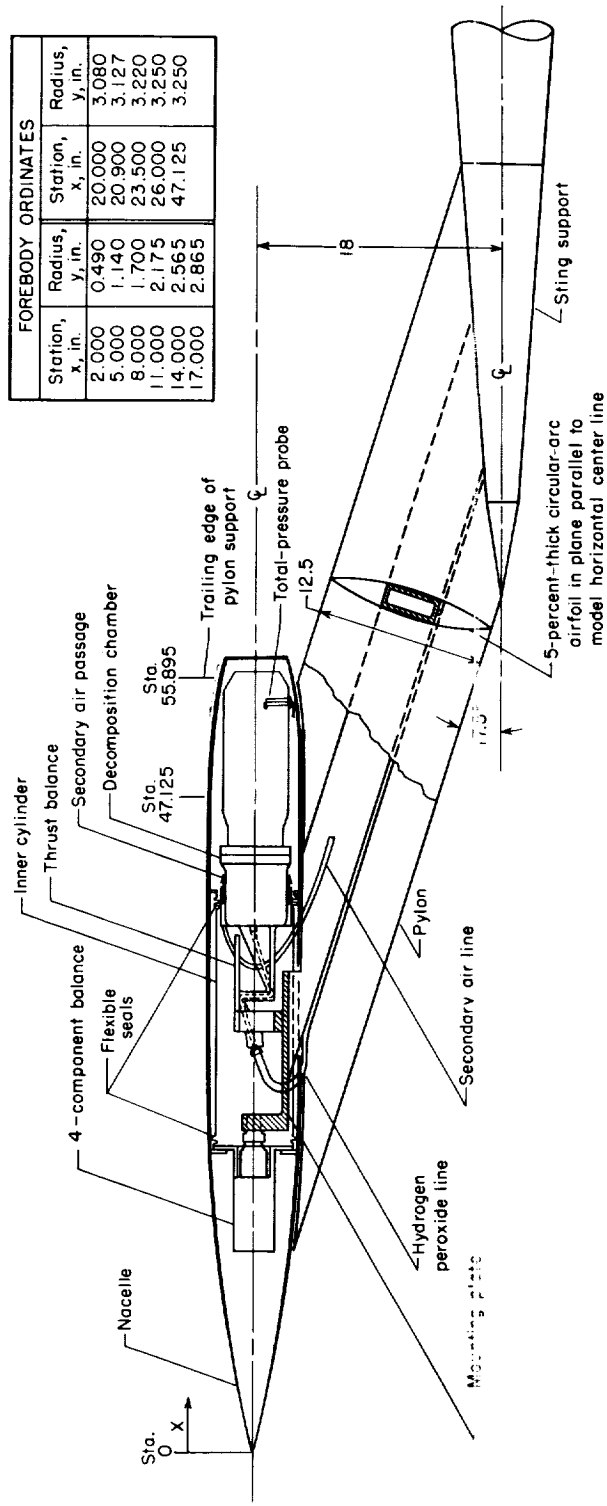


Figure 1.- Sketch of pylon-supported nacelle-jet-simulator model. All dimensions are in inches.

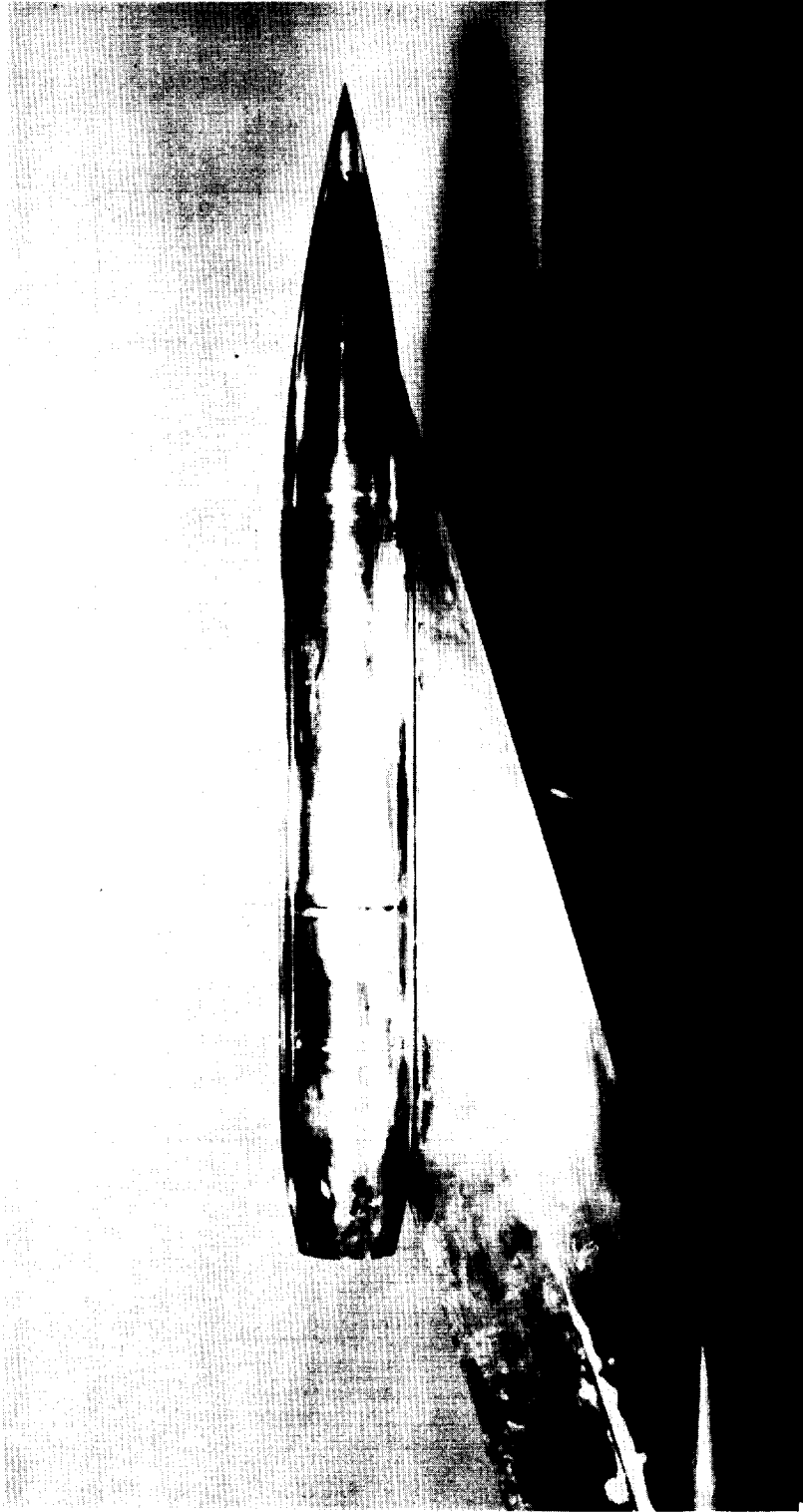
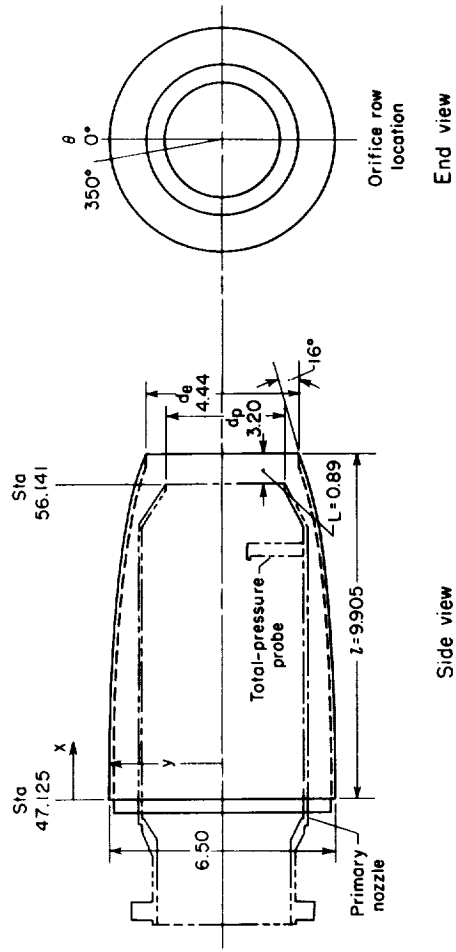


Figure 2.- Photograph of pylon-supported nacelle model with afterbody configuration I. I-58-54



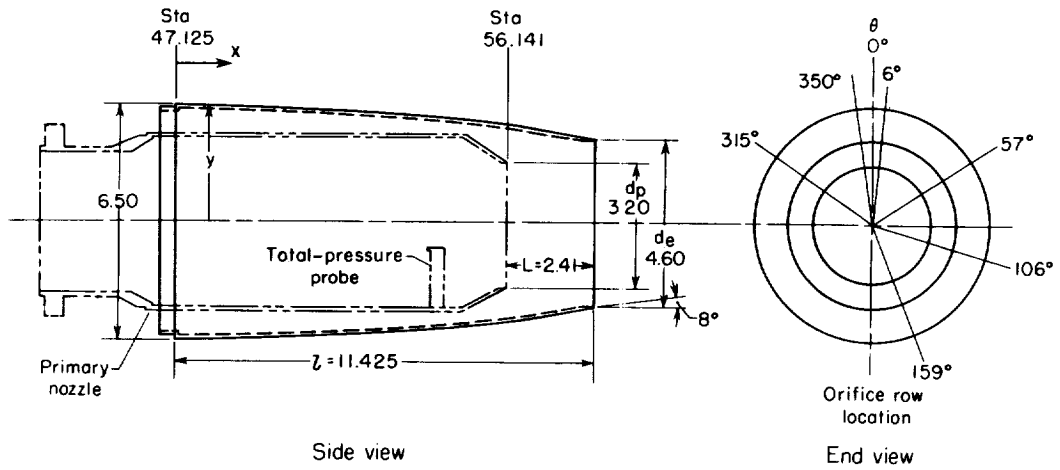
EJECTOR GEOMETRY	
Exit to jet diameter.....	1.367
ratio, d_e/d_p	
Spacing ratio, L/d_p	0.278

EXTERNAL COORDINATES		
Sta	x	y(Radius)
47.125	0.000	3.250
49.061	1.936	3.250
50.260	3.135	3.233
51.260	4.135	3.190
52.260	5.135	3.123
53.260	6.135	3.011
54.460	7.335	2.840
55.260	8.135	2.684
56.260	9.135	2.448
56.760	9.635	2.320
57.030	9.905	2.255

ORIFICE LOCATIONS					
EXTERNAL			INTERNAL		
Row	θ	x	x/L	x	x/L
0	0°	0.475	0.048	4.900	0.495
3	350°	3.475	.351	7.200	.727
4	350°	4.722	.477	8.270	.835
5	350°	5.970	.603	9.300	.939
7	350°	7.484	.756		
8	350°	8.227	.831		
9	350°	8.969	.906		
9	350°	9.722	.982		

(a) Configuration I.

Figure 3.- Sketch of afterbody configurations and locations of pressure orifices. All dimensions are in inches.



EJECTOR GEOMETRY	
Exit to jet diameter.....	1.437
ratio, d_e/d_p	
Spacing ratio, L/d_p	0.753

EXTERNAL COORDINATES		
Sta	x	y(Radius)
47.125	0.000	3.250
48.260	1.135	3.238
50.260	3.135	3.175
52.260	5.135	3.055
53.260	6.135	2.975
54.460	7.335	2.860
55.260	8.135	2.772
56.260	9.135	2.650
57.030	9.905	2.546
57.260	10.135	2.514
58.260	11.135	2.373
58.550	11.425	2.333

ORIFICE LOCATIONS					
EXTERNAL			INTERNAL		
	x	x/L			
Row $\theta = 6^\circ, 57^\circ,$ $106^\circ, 159^\circ$ and 315°	0.480	0.042	Row $\theta = 350^\circ$	4.905	0.430
	3.472	.304		7.205	.631
	4.728	.414		8.275	.725
	5.973	.523		9.305	.815
	7.469	.654			
	8.222	.720			
	8.976	.786			
	9.730	.852			
	10.221	.895			
	11.249	.985			

(c) Configuration III.

Figure 3.- Concluded.

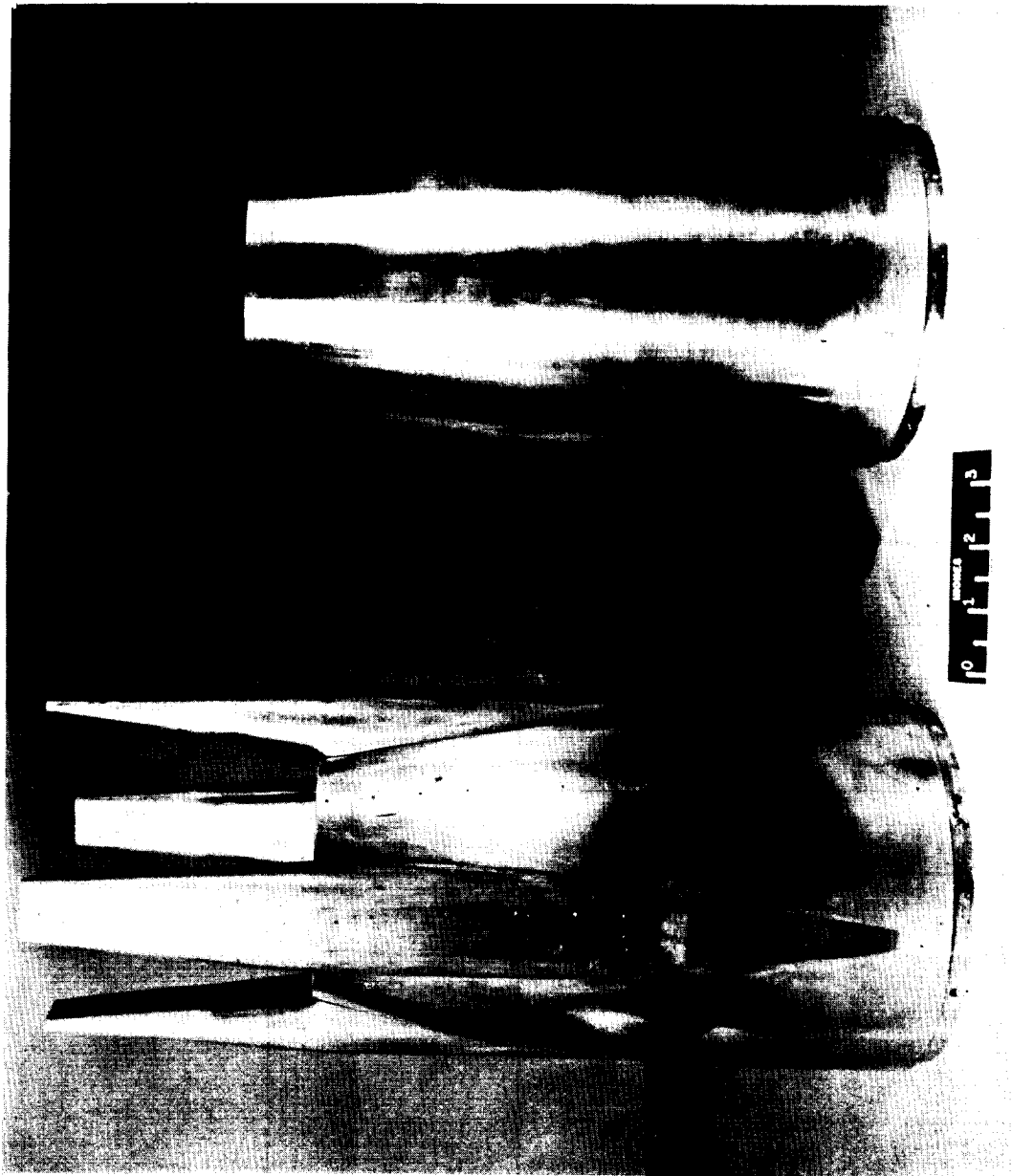


Figure 4.- Photograph of afterbody configurations II and III. L-58-3491

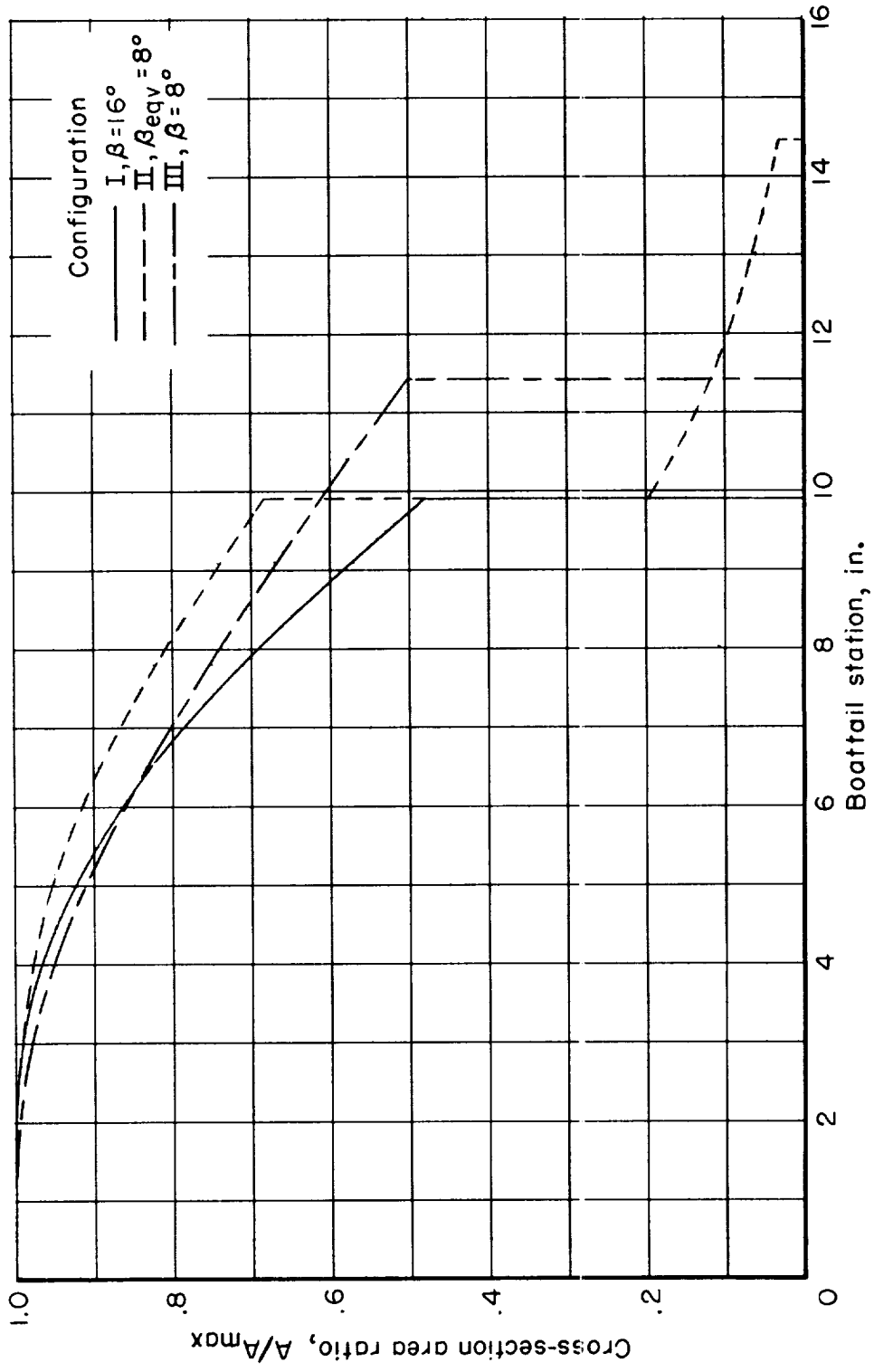


Figure 5.- Area progression of afterbody configurations.

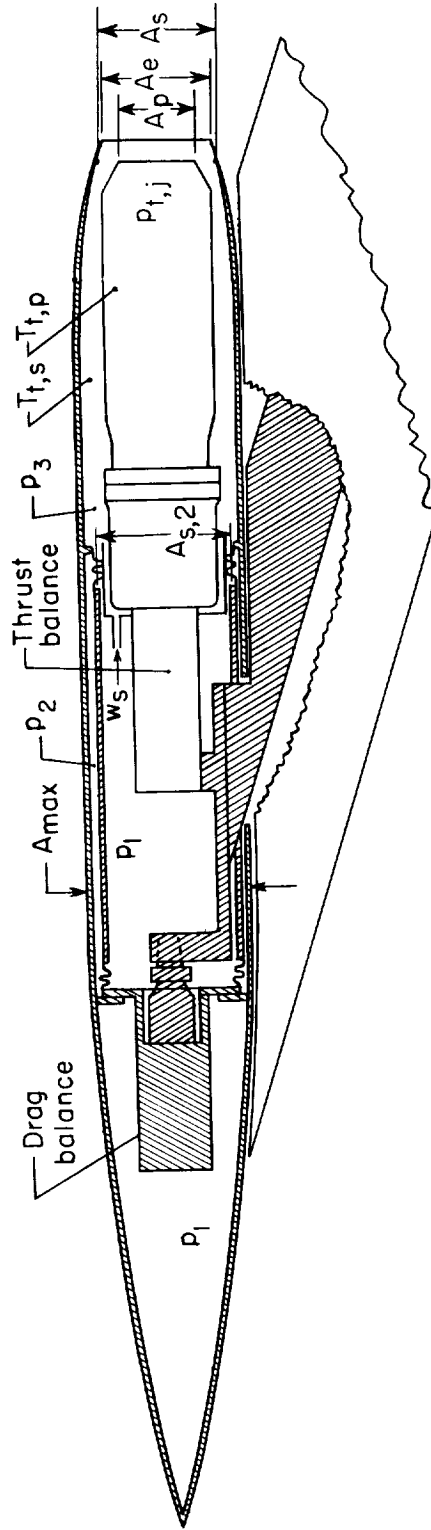
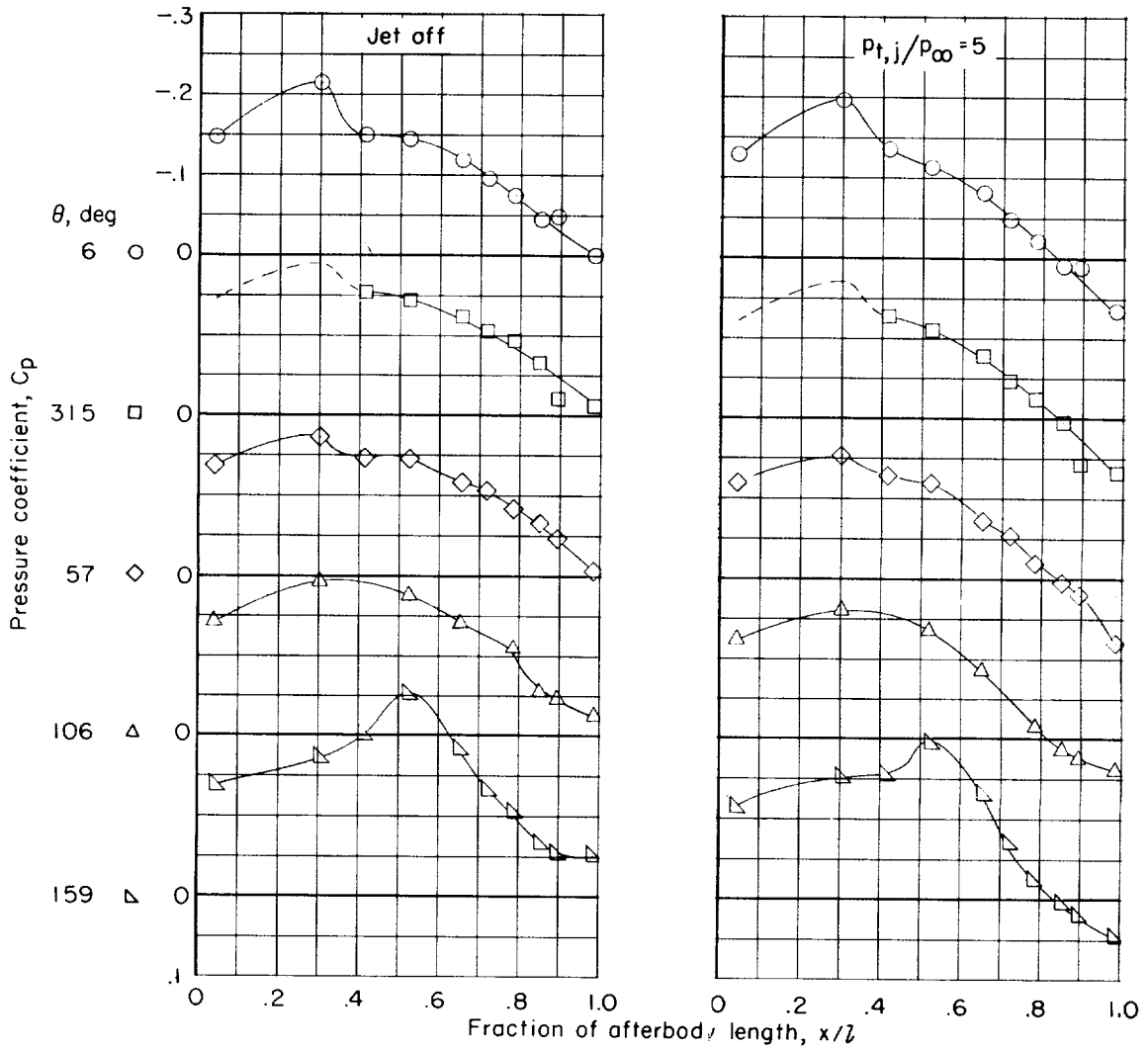
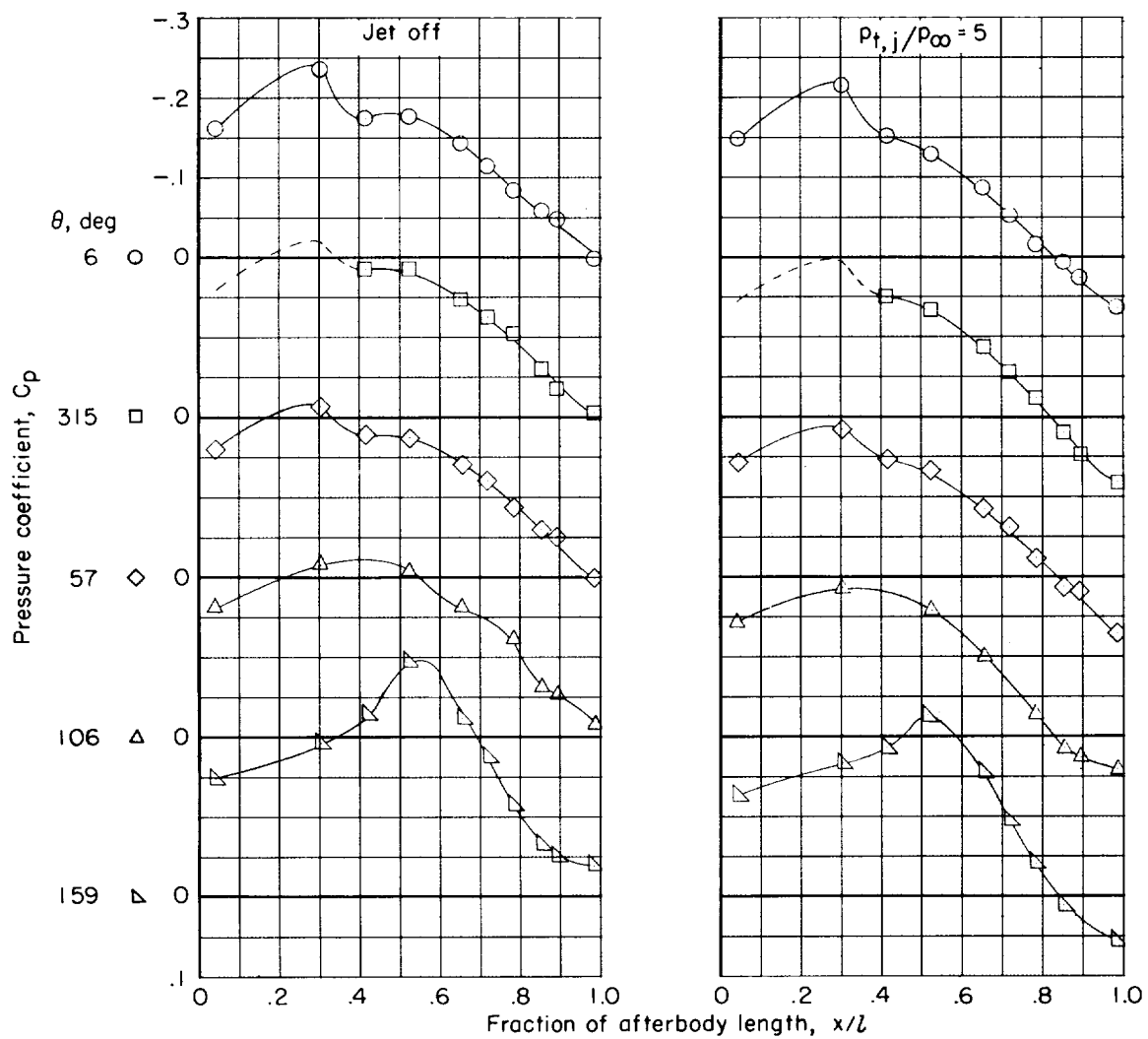


Figure 6.- Schematic diagram showing thrust and drag systems.



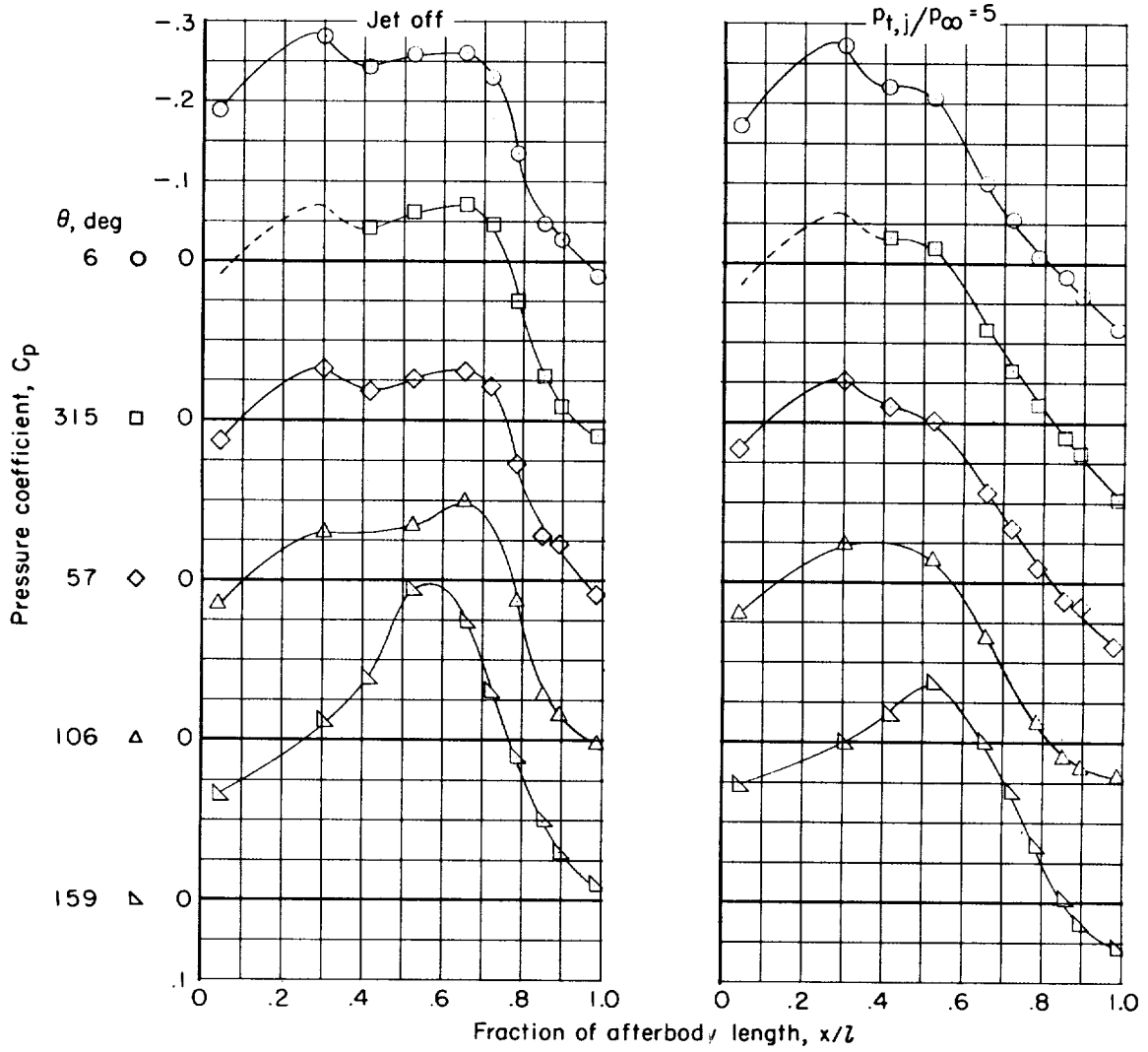
(a) $M = 0.80$.

Figure 7.- Effect of jet operation on pressure distributions of configuration III.



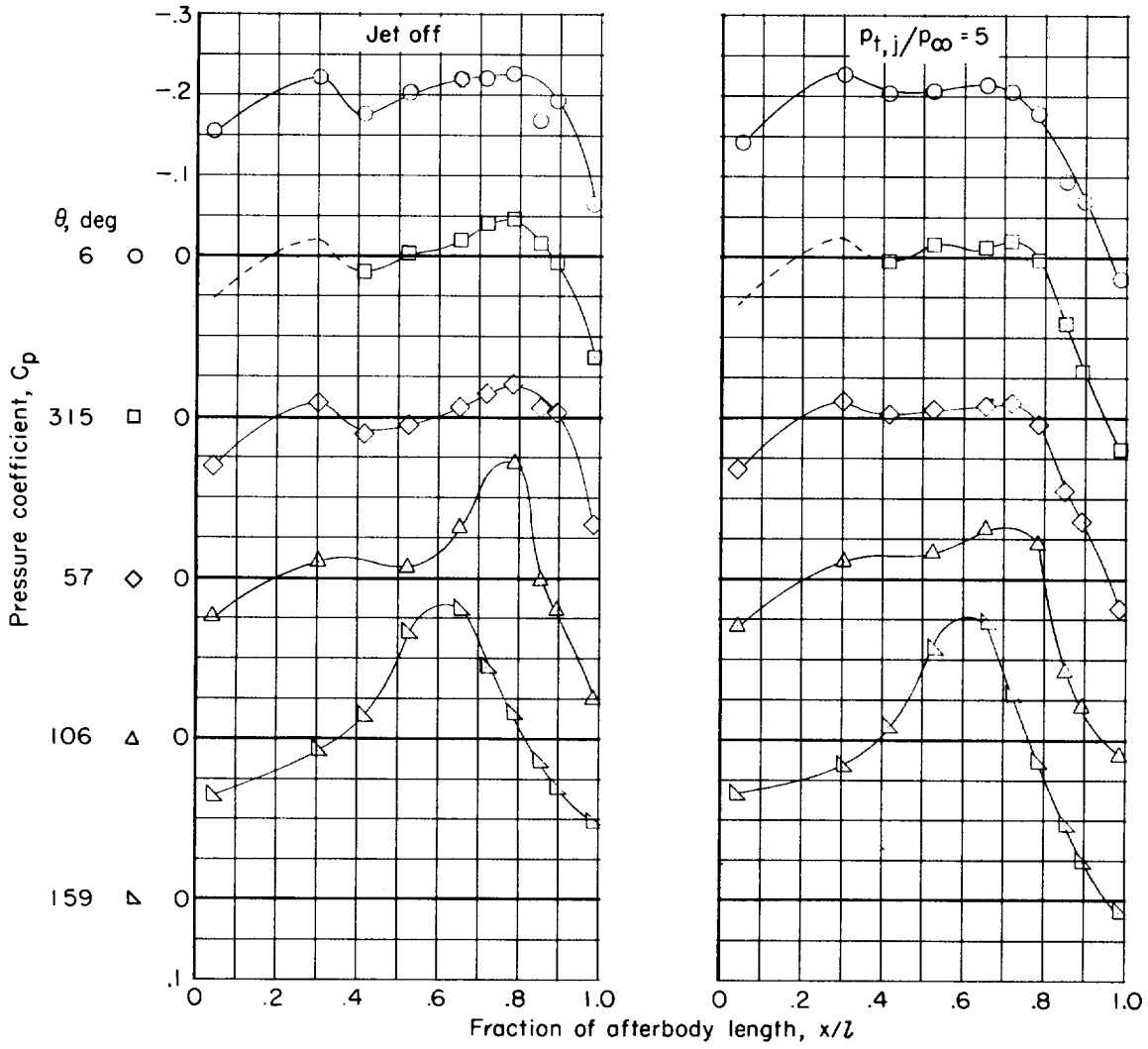
(b) $M = 0.90$.

Figure 7.- Continued.



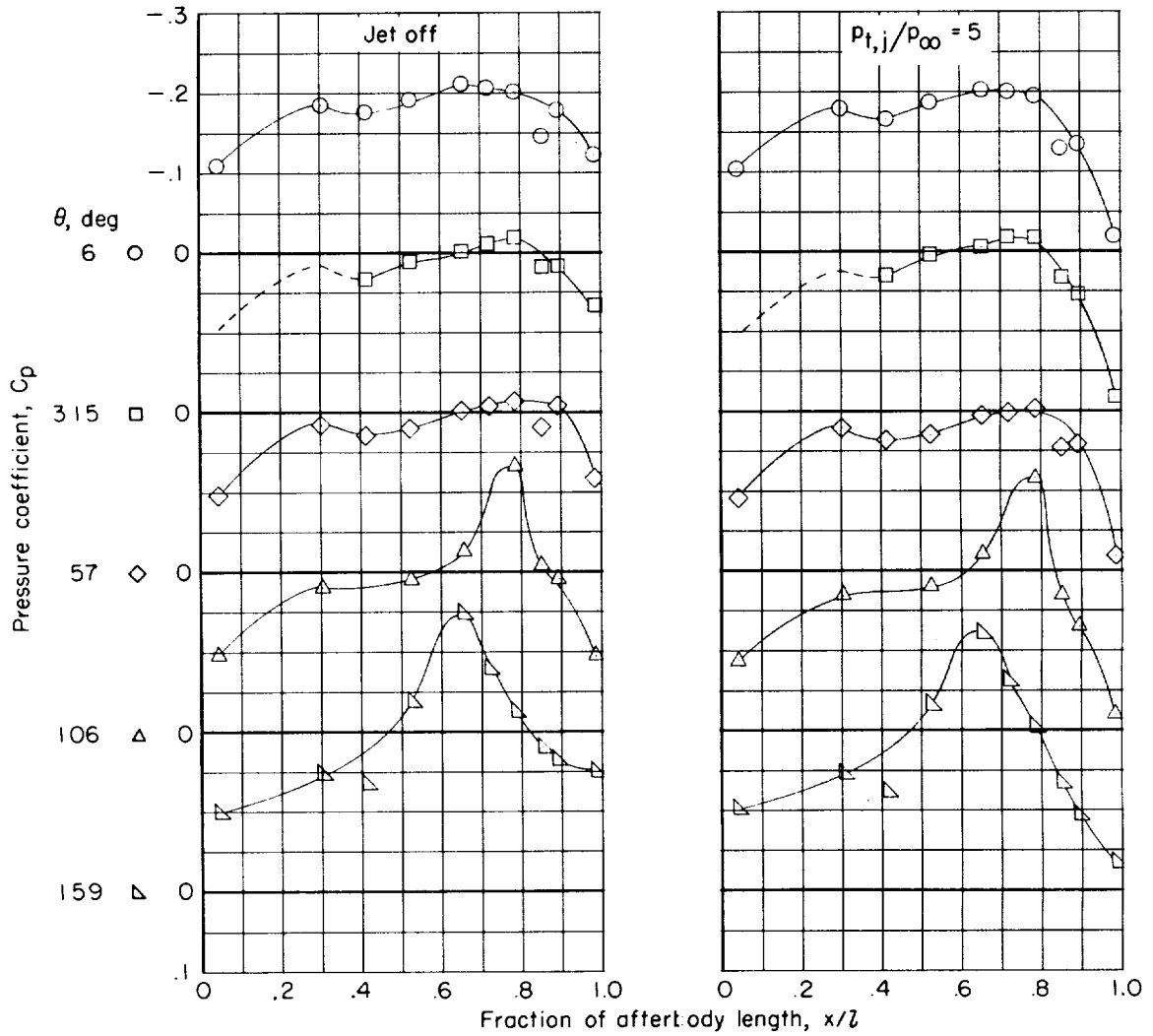
(c) $M = 0.95$.

Figure 7.- Continued.



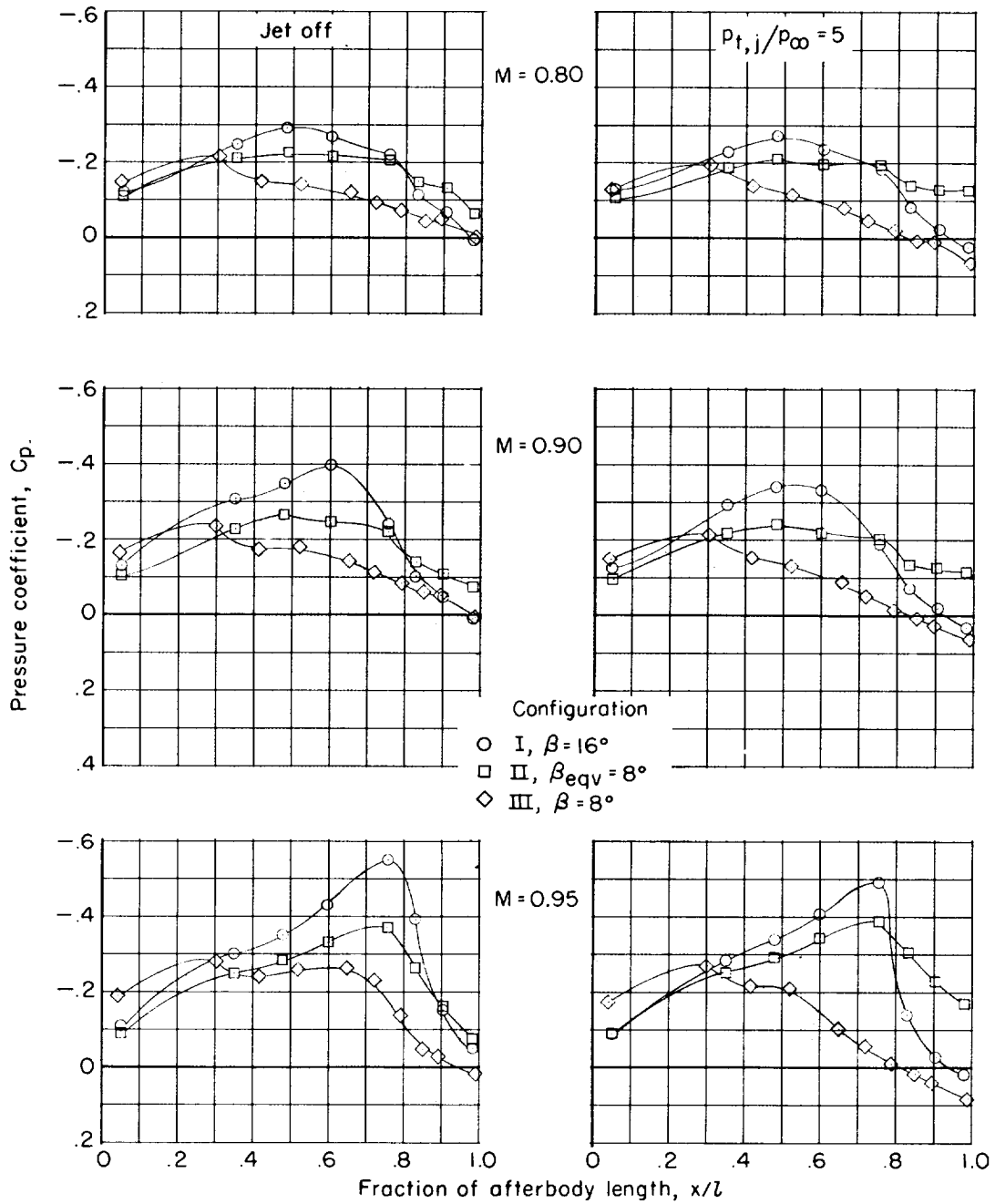
(d) $M = 1.00$.

Figure 7.- Continued.



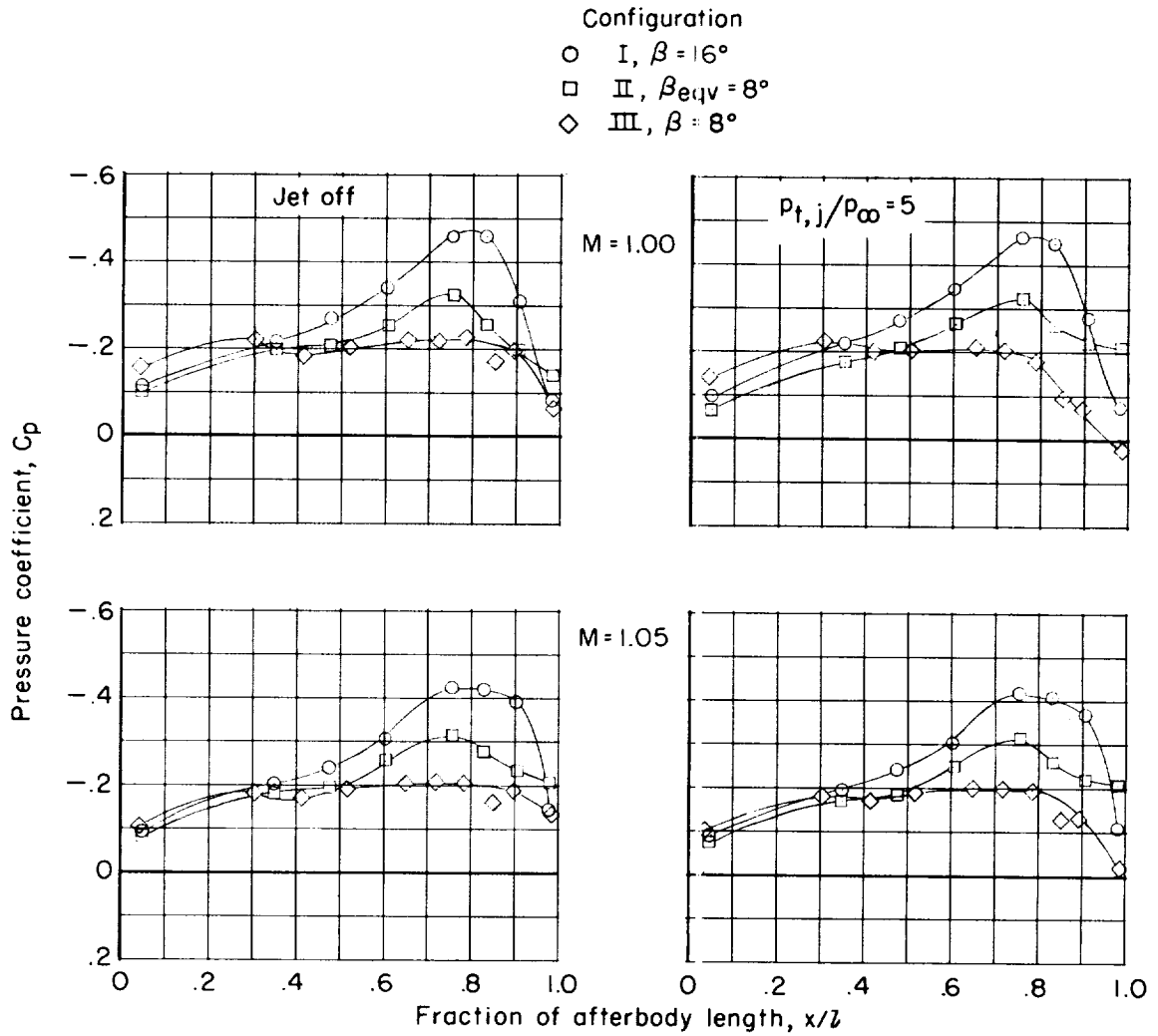
(e) $M = 1.05$.

Figure 7.- Concluded.



(a) $M = 0.80, 0.90, \text{ and } 0.95$.

Figure 8.- Comparisons of pressure distributions for the afterbody configurations tested. $\theta \approx 0^\circ$.



(b) $M = 1.00$ and 1.05 .

Figure 8.- Concluded.

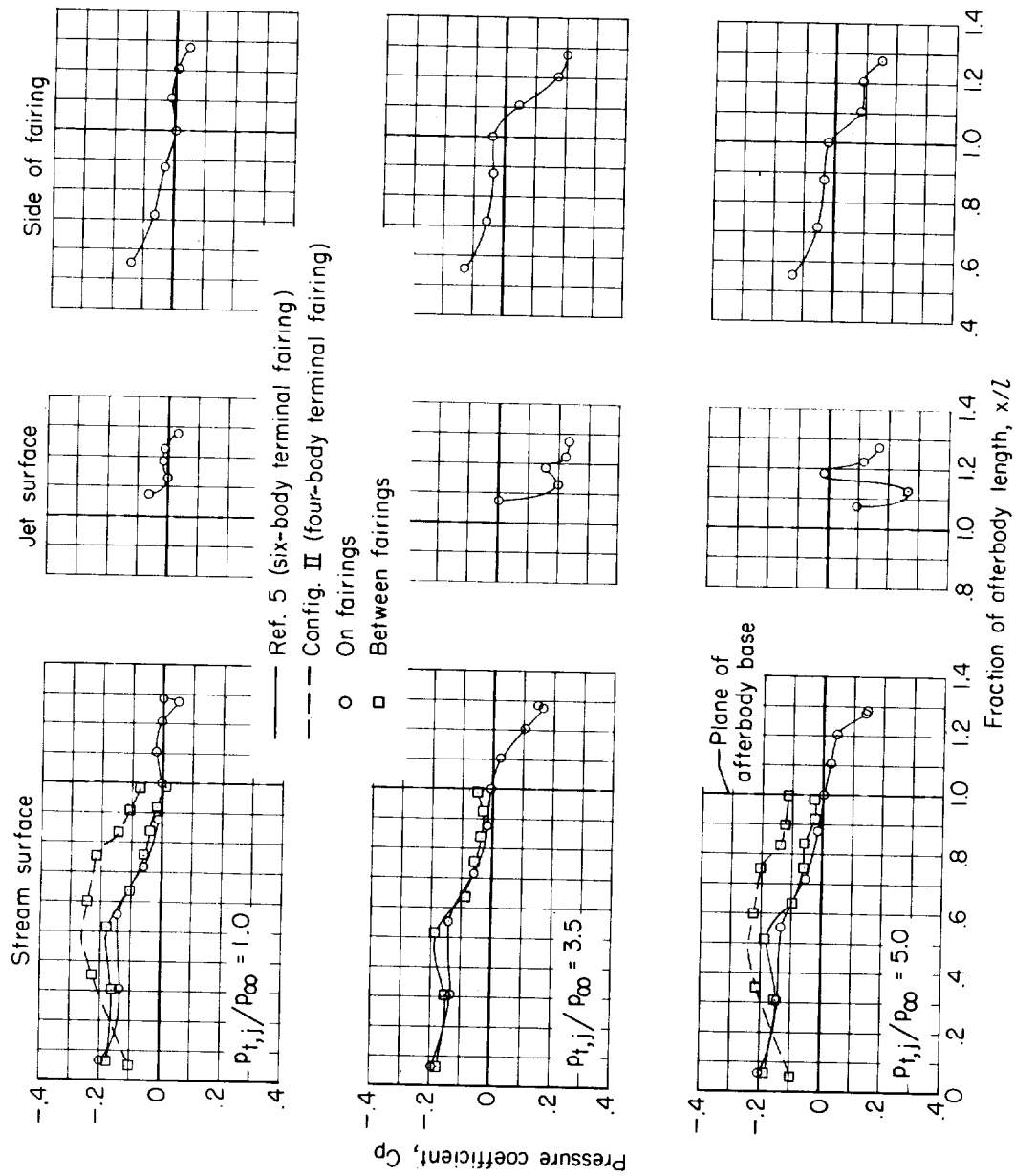


Figure 9.- Effect of jet total-pressure ratio on the pressure distributions obtained over the six-body terminal-fairing configuration of reference 5. $M = 0.90$.

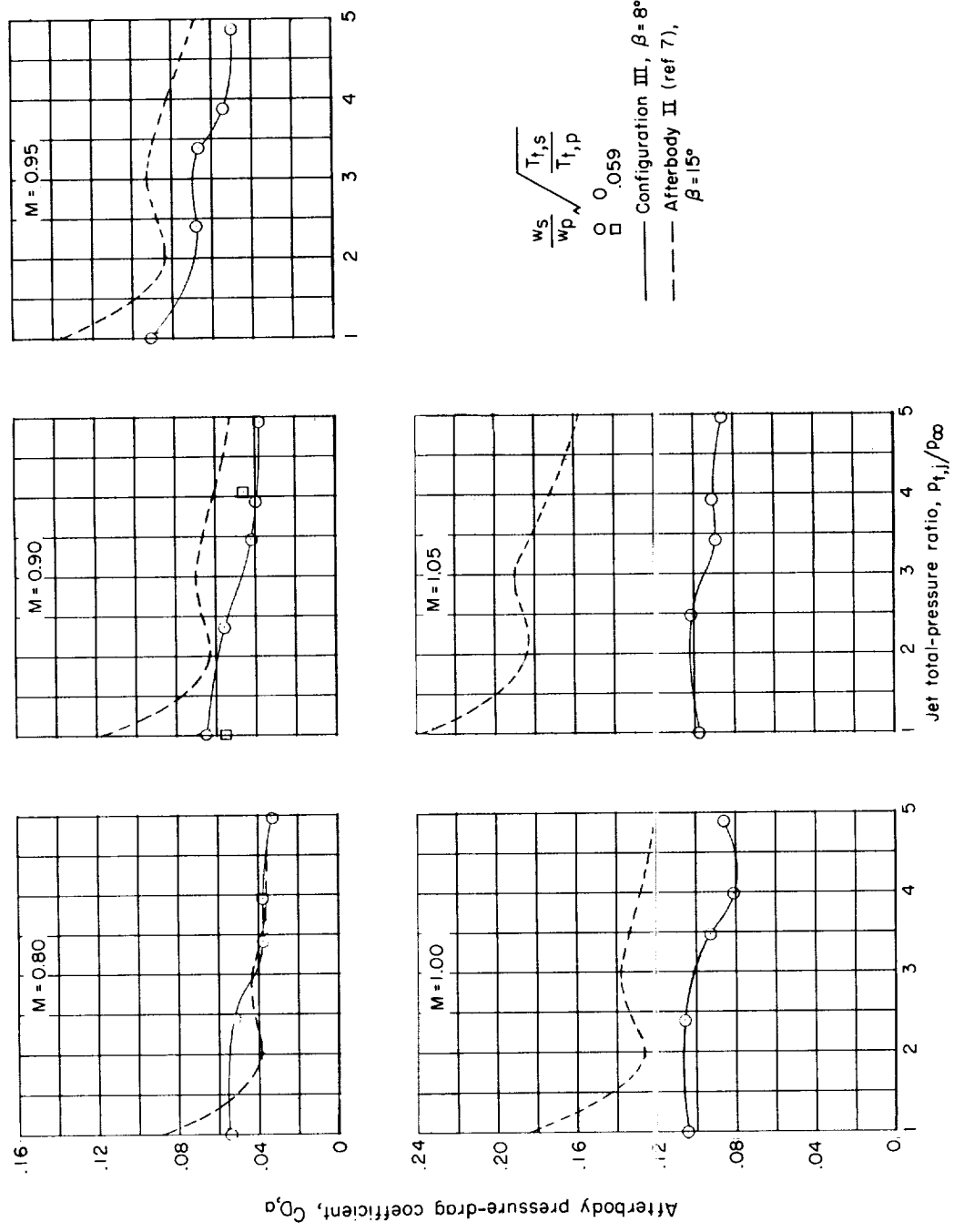


Figure 10.- Variation of afterbody pressure-drag coefficient with jet total-pressure ratio for configuration III.

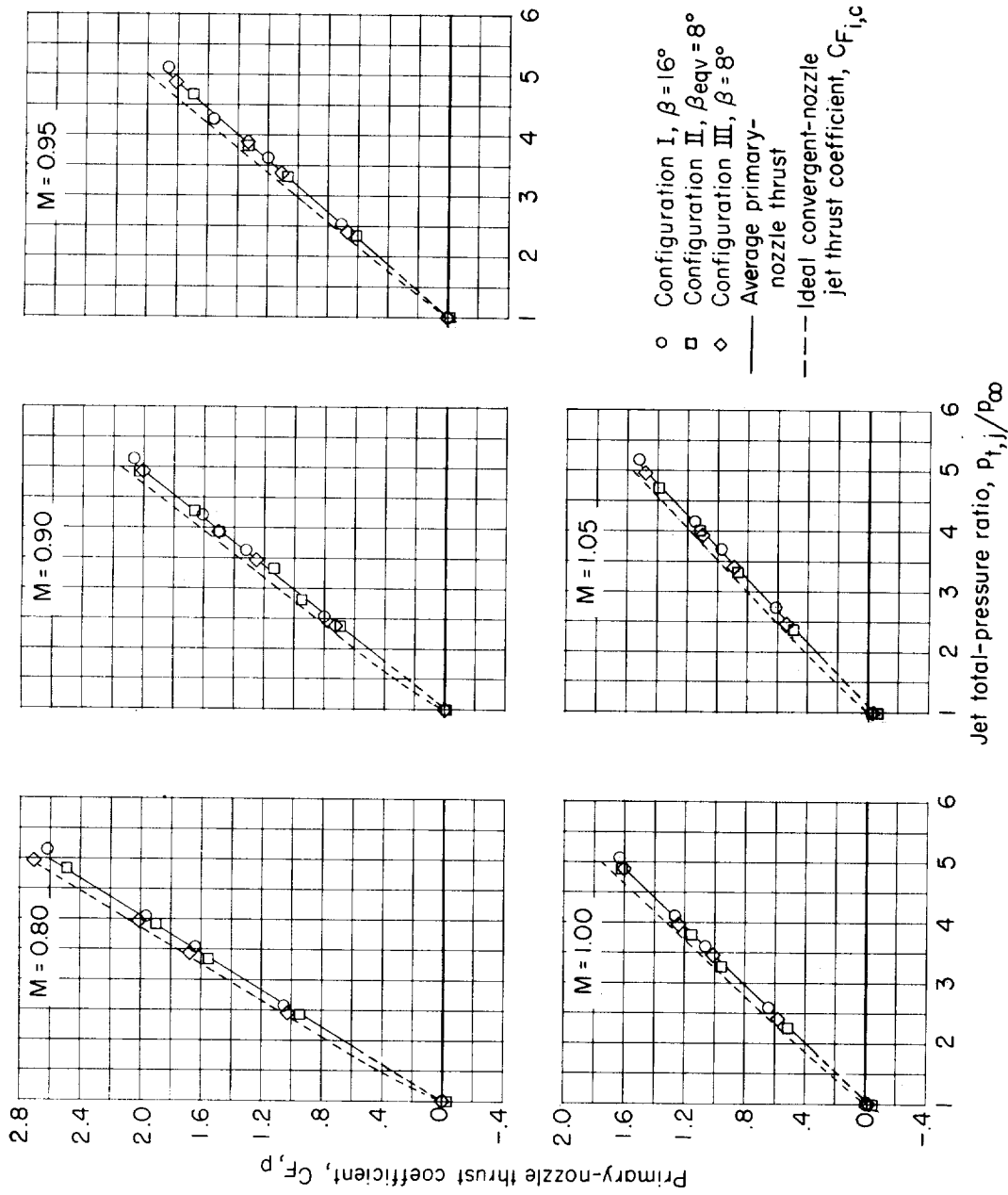


Figure 11.- Variation of primary-nozzle thrust coefficient with jet total-pressure ratio.

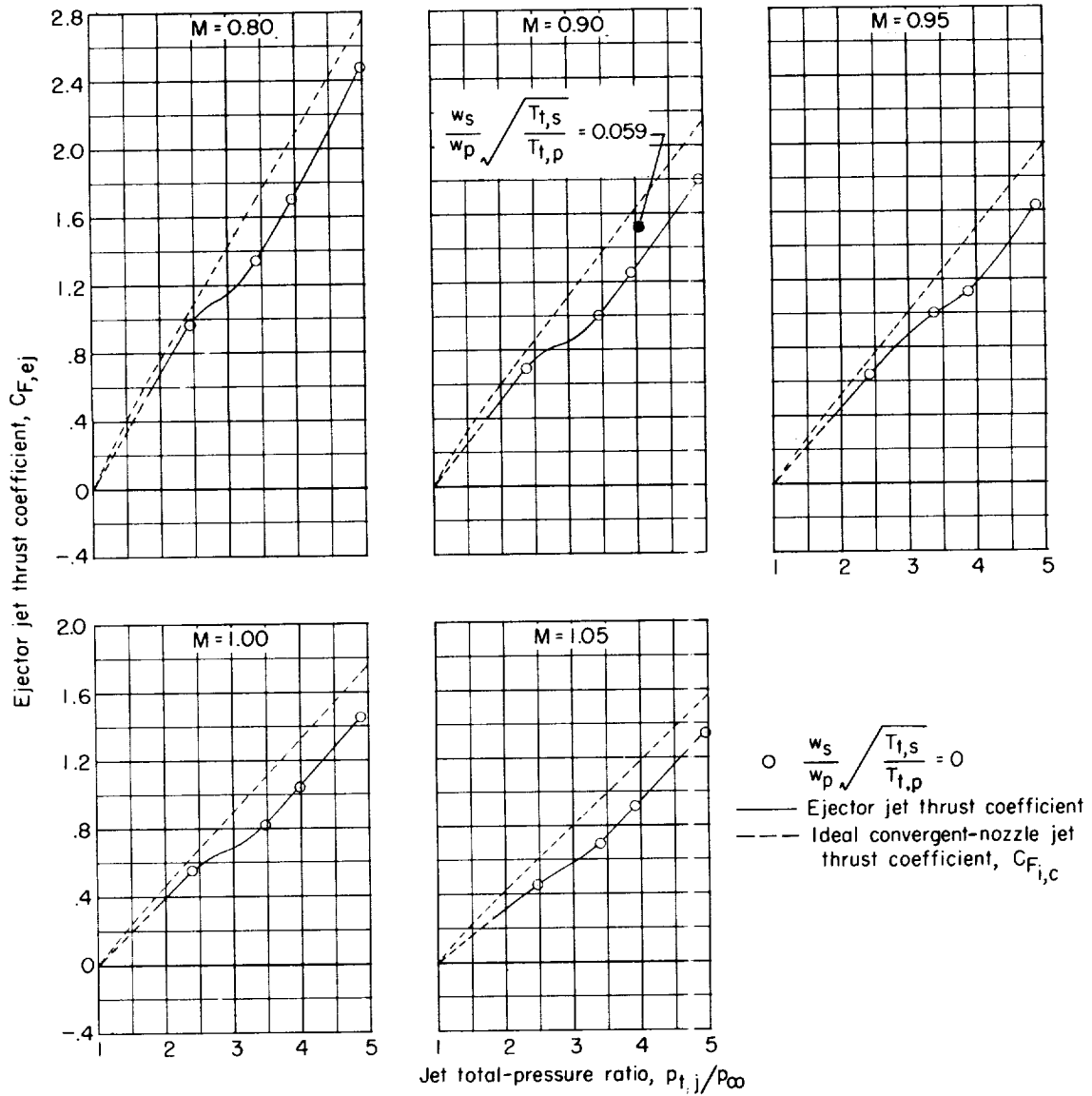


Figure 12.- Variation of ejector jet-thrust coefficient with jet total-pressure ratio for afterbody configuration III. $w_s = 0$.

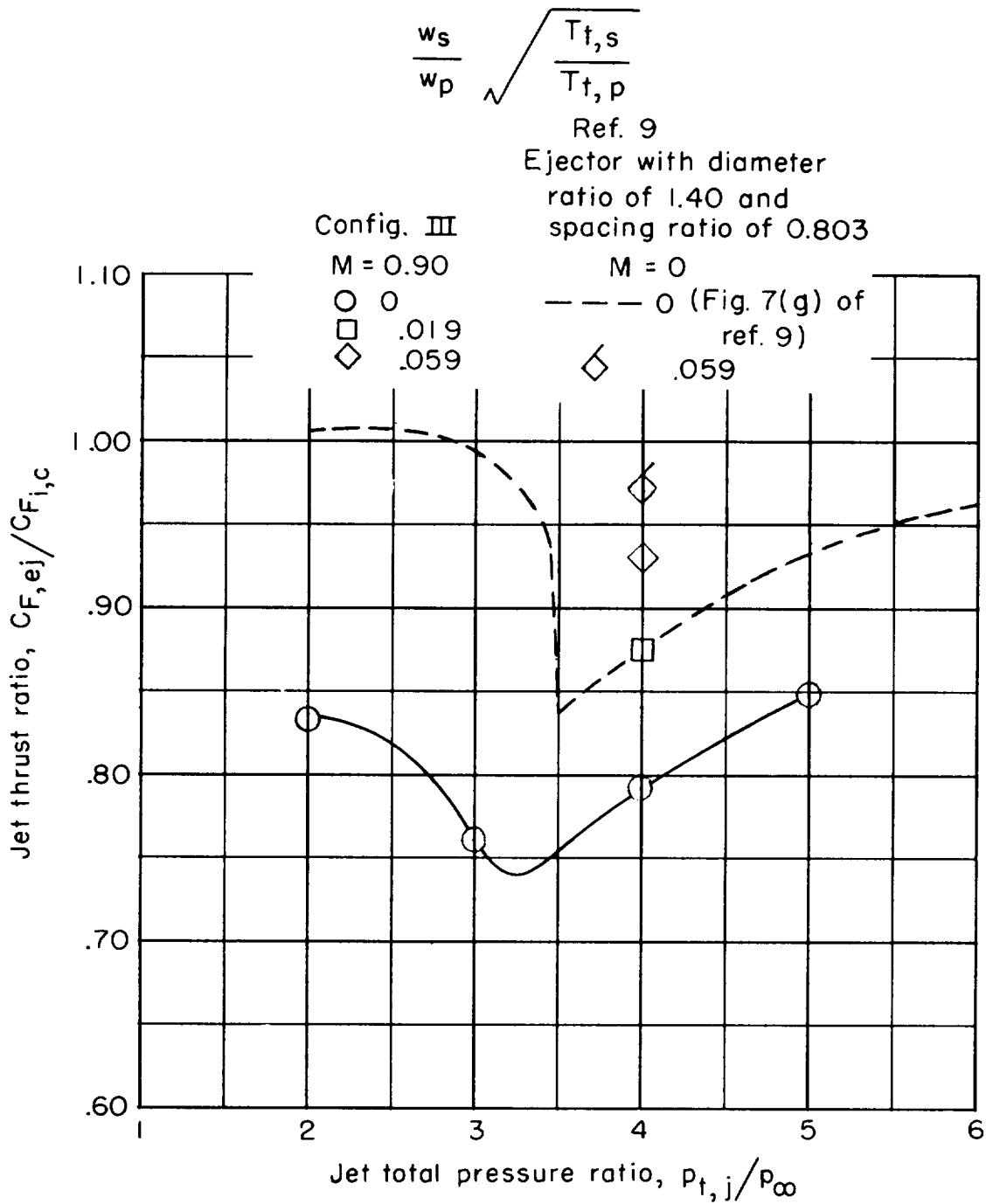


Figure 13.- Effect of secondary to primary weight flow ratio on jet thrust ratio for afterbody configuration III.

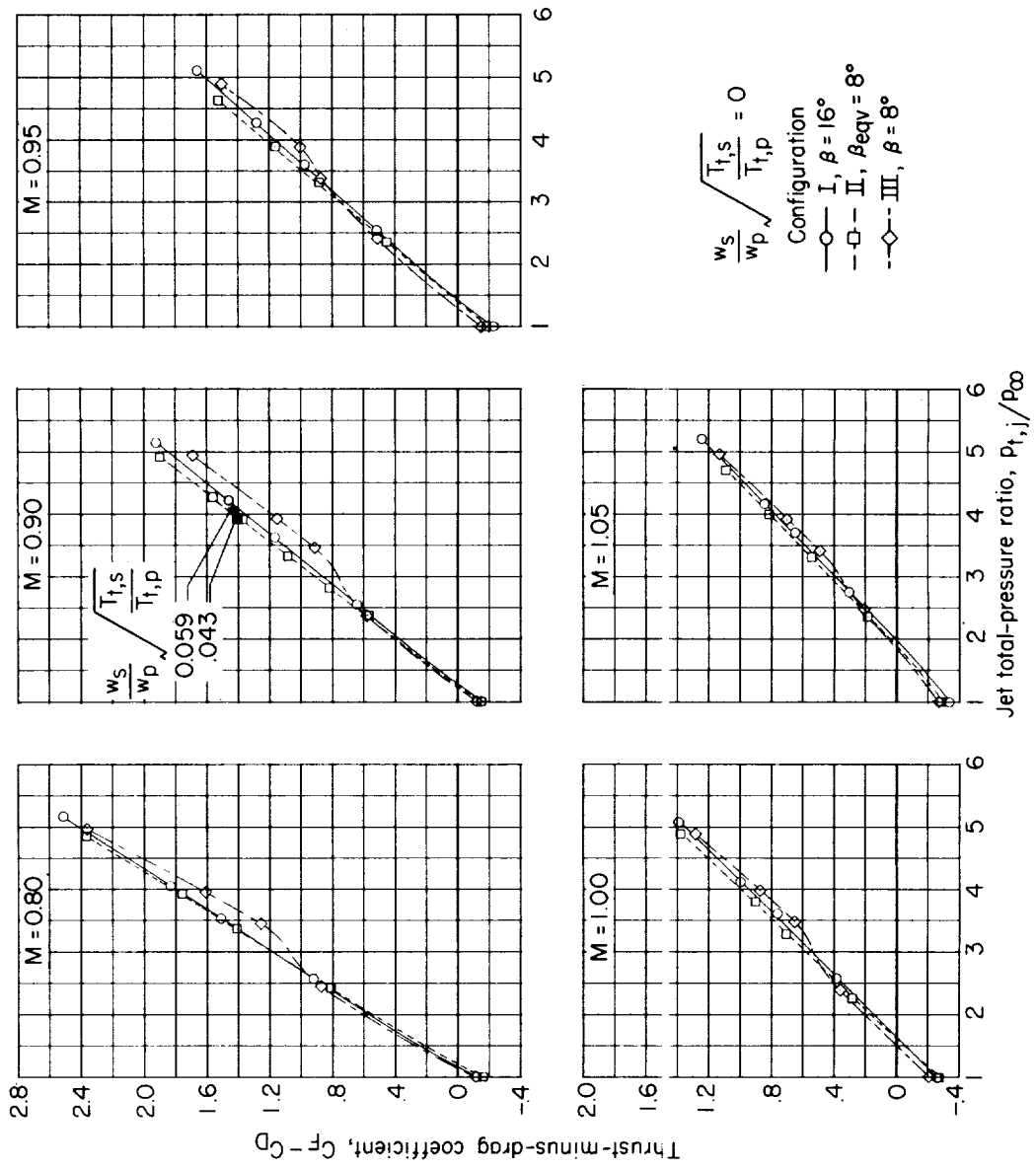


Figure 14.- Variation of thrust-minus-drag coefficient with jet total-pressure ratio for the afterbody models.

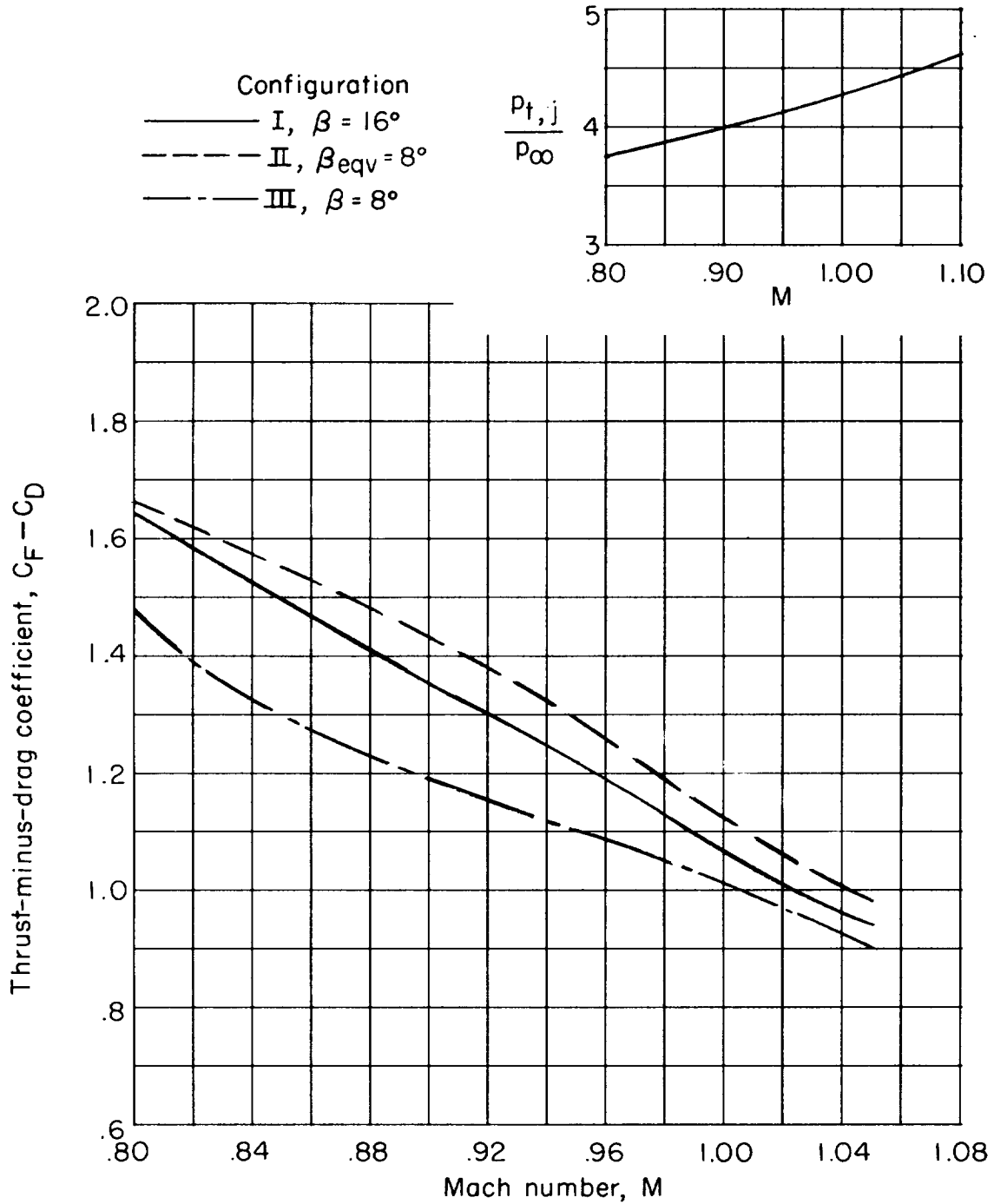


Figure 15.- Variation of thrust-minus-drag coefficient with Mach number for the different afterbodies at a scheduled pressure ratio. $w_s = 0$.

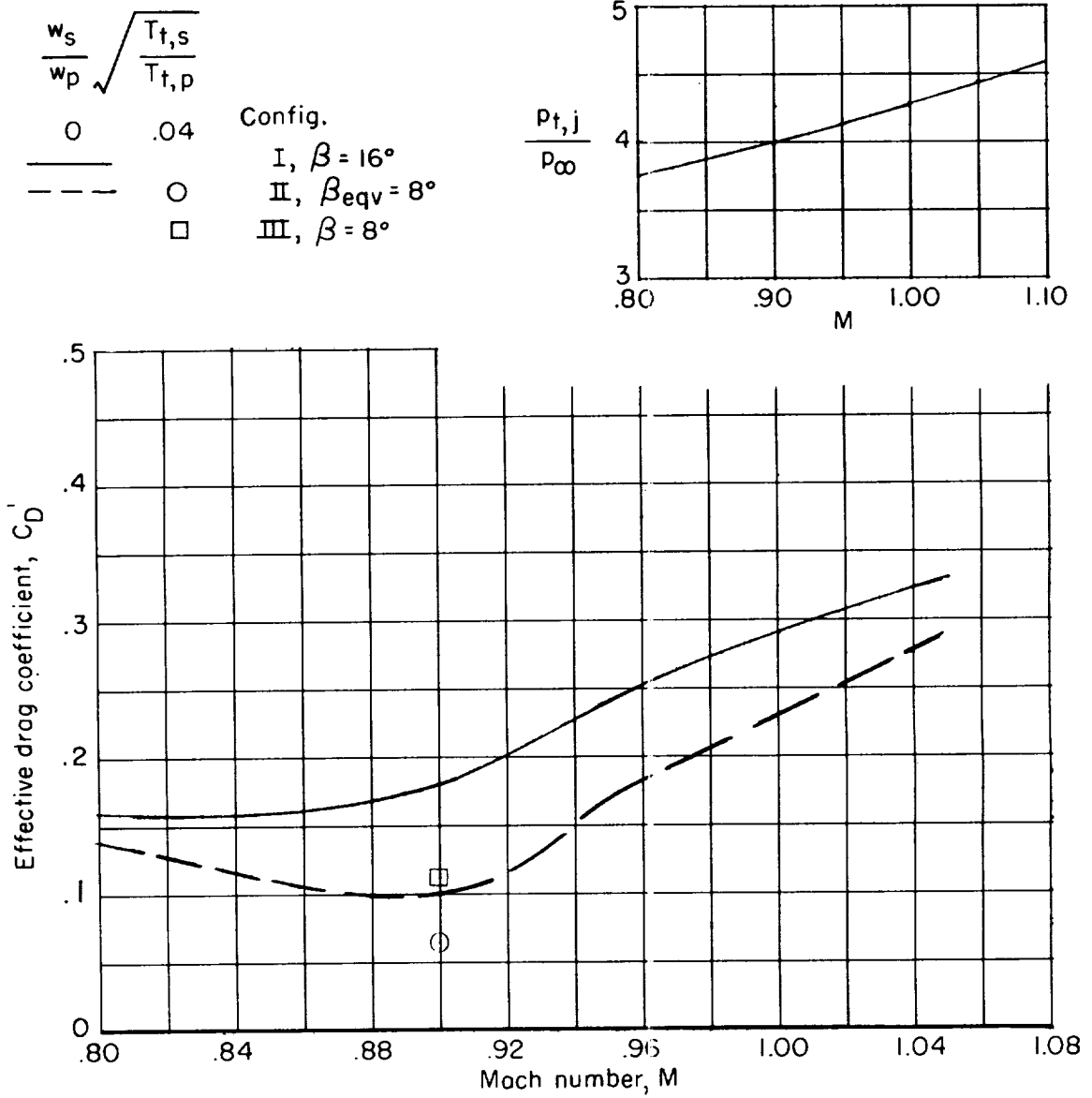


Figure 16.- Variation of effective drag coefficient with Mach number for the different afterbodies at a scheduled jet total-pressure ratio.

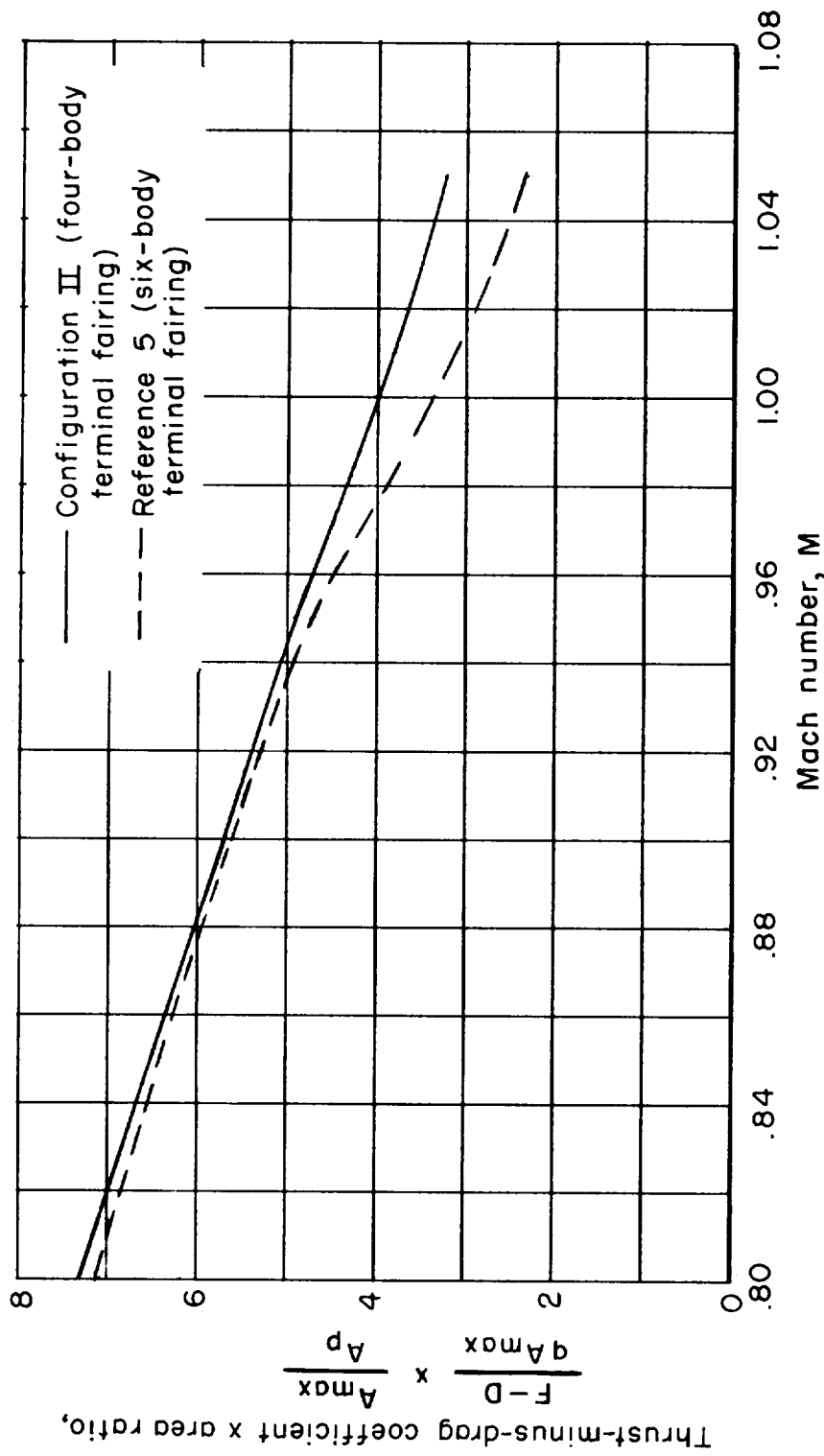


Figure 17.- Comparison of thrust-minus-drag coefficient for two terminal-fairing configurations over the Mach number range at a jet total-pressure ratio of 4. $w_s/w_p = 0$.

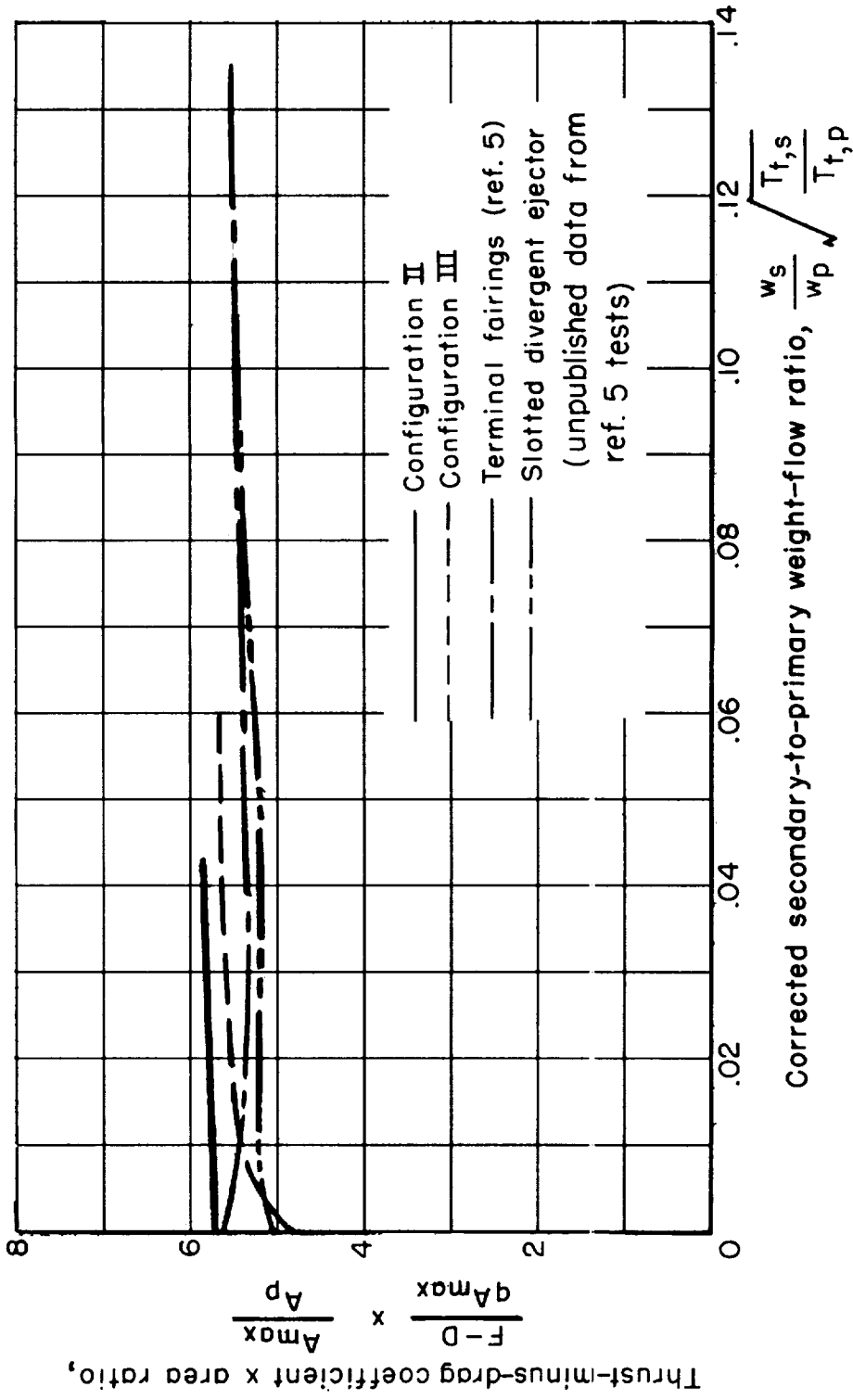


Figure 18.- Comparison of thrust-minus-drag coefficient for four afterbody configurations with corrected secondary weight flow ratios at a Mach number of 0.90 and a jet total-pressure ratio of 4.

NASA TM X-215

National Aeronautics and Space Administration.
EFFECT OF AFTERBODY TERMINAL FAIRINGS ON
THE PERFORMANCE OF A PYLON-MOUNTED
TURBOJET-NACELLE MODEL. Conrad M. Willis
and Charles E. Mercer. March 1960. 38p.
diags., photos.
(NASA TECHNICAL MEMORANDUM X-215)

(Title, Unclassified)
Three simulated turbojet-nacelle configurations were tested; two were simple bodies of revolution with boattail angles of 8° and 16° and the third was a terminal-fairing configuration with an equivalent boattail angle of 8°. The tests were conducted at 0° angle of attack with the use of a hot-jet exhaust at jet total-pressure ratios of 1 to 5 over a Mach number range of 0.80 to 1.05. The addition of terminal fairings increased the thrust-minus-drag coefficients of the afterbody throughout the Mach number range.

1. Flow, Jet-Mixing (1.1.3.3)
 2. Bodies - Shape Variables (1.3.2)
 3. Exits (1.4.3)
 4. Interference, Jet - Airplanes (1.7.1.1.6)
 5. Airplanes - Performance (1.7.1.3)
- I. Willis, Conrad M.
 - II. Mercer, Charles E.
 - III. NASA TM X-215

NASA

NASA TM X-215

National Aeronautics and Space Administration.
EFFECT OF AFTERBODY TERMINAL FAIRINGS ON
THE PERFORMANCE OF A PYLON-MOUNTED
TURBOJET-NACELLE MODEL. Conrad M. Willis
and Charles E. Mercer. March 1960. 38p.
diags., photos.
(NASA TECHNICAL MEMORANDUM X-215)

(Title, Unclassified)
Three simulated turbojet-nacelle configurations were tested; two were simple bodies of revolution with boattail angles of 8° and 16° and the third was a terminal-fairing configuration with an equivalent boattail angle of 8°. The tests were conducted at 0° angle of attack with the use of a hot-jet exhaust at jet total-pressure ratios of 1 to 5 over a Mach number range of 0.80 to 1.05. The addition of terminal fairings increased the thrust-minus-drag coefficients of the afterbody throughout the Mach number range.

1. Flow, Jet-Mixing (1.1.3.3)
 2. Bodies - Shape Variables (1.3.2)
 3. Exits (1.4.3)
 4. Interference, Jet - Airplanes (1.7.1.1.6)
 5. Airplanes - Performance (1.7.1.3)
- I. Willis, Conrad M.
 - II. Mercer, Charles E.
 - III. NASA TM X-215

NASA

NASA TM X-215

National Aeronautics and Space Administration.
EFFECT OF AFTERBODY TERMINAL FAIRINGS ON
THE PERFORMANCE OF A PYLON-MOUNTED
TURBOJET-NACELLE MODEL. Conrad M. Willis
and Charles E. Mercer. March 1960. 38p.
diags., photos.
(NASA TECHNICAL MEMORANDUM X-215)

(Title, Unclassified)
Three simulated turbojet-nacelle configurations were tested; two were simple bodies of revolution with boattail angles of 8° and 16° and the third was a terminal-fairing configuration with an equivalent boattail angle of 8°. The tests were conducted at 0° angle of attack with the use of a hot-jet exhaust at jet total-pressure ratios of 1 to 5 over a Mach number range of 0.80 to 1.05. The addition of terminal fairings increased the thrust-minus-drag coefficients of the afterbody throughout the Mach number range.

1. Flow, Jet-Mixing (1.1.3.3)
 2. Bodies - Shape Variables (1.3.2)
 3. Exits (1.4.3)
 4. Interference, Jet - Airplanes (1.7.1.1.6)
 5. Airplanes - Performance (1.7.1.3)
- I. Willis, Conrad M.
 - II. Mercer, Charles E.
 - III. NASA TM X-215

NASA

NASA TM X-215

National Aeronautics and Space Administration.
EFFECT OF AFTERBODY TERMINAL FAIRINGS ON
THE PERFORMANCE OF A PYLON-MOUNTED
TURBOJET-NACELLE MODEL. Conrad M. Willis
and Charles E. Mercer. March 1960. 38p.
diags., photos.
(NASA TECHNICAL MEMORANDUM X-215)

(Title, Unclassified)
Three simulated turbojet-nacelle configurations were tested; two were simple bodies of revolution with boattail angles of 8° and 16° and the third was a terminal-fairing configuration with an equivalent boattail angle of 8°. The tests were conducted at 0° angle of attack with the use of a hot-jet exhaust at jet total-pressure ratios of 1 to 5 over a Mach number range of 0.80 to 1.05. The addition of terminal fairings increased the thrust-minus-drag coefficients of the afterbody throughout the Mach number range.

1. Flow, Jet-Mixing (1.1.3.3)
 2. Bodies - Shape Variables (1.3.2)
 3. Exits (1.4.3)
 4. Interference, Jet - Airplanes (1.7.1.1.6)
 5. Airplanes - Performance (1.7.1.3)
- I. Willis, Conrad M.
 - II. Mercer, Charles E.
 - III. NASA TM X-215

NASA

